FIBER LASER ARRAY

Thomas B. Simpson

The Titan Corporation
Applied Technology Sector
3394 Carmel Mountain Road
San Diego, CA 92121

January 2004

Final Report

AIR FORCE RESEARCH LABORATORY
Directed Energy Directorate
3550 Aberdeen Ave SE
AIR FORCE MATERIEL COMMAND
KIRTLAND AIR FORCE BASE, NM 87117-5776

DTIC COPY

This report has been reviewed by the Public Affairs office and is releasable to the National Technical Information Service (NTIS). At NTIS, it will be available to the general public, including foreign nationals.

If you change your address, wish to be removed from this mailing list, or your organization no longer employs the addressee, please notify AFRL/DELO, 3550 Aberdeen Ave SE, Kirtland AFB, NM 87117-5776.

Do not return copies of this report unless contractual obligations or notice on a specific document requires its return.

This report has been approved for publication.

//signed//

PHILLIP R. PETERSON, PhD, DR-III
Project Manager

//signed//

LEANN D. BRASURE, Lt Col, USAF

//signed//

L. BRUCE SIMPSON, SES

Chief, High Power Solid State Lasers Branch

Director, Directed Energy Directorate

REPORT DOCUMENTATION PAGE

Form Approved
OMB No. 0704-0188

1. REPORT DATE *(DD-MM-YYYY)*	2. REPORT TYPE	3. DATES COVERED *(From - To)*
30-01-2004	Final Technical Report	February 2002 – December 2003

4. TITLE AND SUBTITLE

Fiber Laser Array

5a. CONTRACT NUMBER
F29601-01-C-0233

5b. GRANT NUMBER

5c. PROGRAM ELEMENT NUMBER
62605F

6. AUTHOR(S)
Thomas B. Simpson

5d. PROJECT NUMBER
4866

5e. TASK NUMBER
LR

5f. WORK UNIT NUMBER
02

7. PERFORMING ORGANIZATION NAME(S) AND ADDRESS(ES)

The Titan Corporation
Applied Technology Sector
3394 Carmel Mountain Road
San Diego, CA 92121

8. PERFORMING ORGANIZATION REPORT NUMBER

D04-018

9. SPONSORING / MONITORING AGENCY NAME(S) AND ADDRESS(ES)

AFRL/DELO
3550 Aberdeen Ave. SE
Kirtland AFB, NM 87117-5776

10. SPONSOR/MONITOR'S ACRONYM(S)

11. SPONSOR/MONITOR'S REPORT NUMBER(S)
AFRL-DE-PS-TR-2004-1028

12. DISTRIBUTION / AVAILABILITY STATEMENT

Approved for public release; distribution is unlimited.

13. SUPPLEMENTARY NOTES
The views, opinions and/or findings contained in this report are those of the author(s) and should not be construed as an official Department of the Air Force position, policy or decision, unless so designated by other documentation.

14. ABSTRACT

Experiments have been conducted to investigate the feasibility and scalability of coherent laser output from an array of fiber lasers with strong intracavity coupling. A flexible, reconfigurable experimental apparatus has been modified and configured for these investigations. Measurements taken with this apparatus during this program showed that without polarization selection, the lasers were likely to exhibit spectra that showed the effects of polarization mode dispersion. Arrays of 2-5 amplifier elements coupled using the 2×2 fiber couplers were constructed with emphasis on a unidirectional ring configuration. A theoretical prediction that for a range of pump powers more power can be coherently coupled out of an array than is available at all outputs of an incoherently coupled array was verified experimentally. A novel pulsating behavior was observed over a range of operating conditions for the two-element array. An extensive series of runs was made where the overall cavity length or the lengths of individual element paths were varied over a wide range. Stable output from a four-laser array could only be observed when there was significant length mismatch between the array elements. Spectral features related to the mismatch in cavity length for the array elements were identified. A transition in the spectral characteristics indicated that cross coupling between optical modes was the first significant nonlinear optical interaction in the array. There appears to be a complex interplay between the spectral

15. SUBJECT TERMS

Coherent Coupling of Lasers	Erbium-doped Fiber Amplifier	Fiber Laser
Laser Array	Nonlinear Dynamics	Nonlinear Optics

16. SECURITY CLASSIFICATION OF:			17. LIMITATION OF ABSTRACT	18. NUMBER OF PAGES	19a. NAME OF RESPONSIBLE PERSON
					Dr. Phillip R. Peterson
a. REPORT	b. ABSTRACT	c. THIS PAGE	Unlimited	64	19b. TELEPHONE NUMBER *(include area code)*
Unclassified	Unclassified	Unclassified			(505) 846-9301

Standard Form 298 (Rev. 8-98)
Prescribed by ANSI Std. Z39.18

(This page intentionally left blank.)

TABLE OF CONTENTS

INTRODUCTION 3

POLARIZATION-RESOLVED MEASUREMENTS AND LINEAR-CAVITY COMPARISONS 6

RING-LASER RECONFIGURATIONS 21

Two-Laser Arrays 27

Four- and Five-Laser Arrays 33

CONCLUSIONS 46

RECOMMENDATIONS 48

REFERENCES 50

LIST OF FIGURES

Figure		Page
1.	Schematic of the basic two-element configuration that demonstrated self-selected coherent output	4
2.	Schematic of the two-laser configuration with the modifications that have been implemented to study issues related to polarization of the optical output and cavity length mismatch	8
3.	Schematic of the optical path outside of the fiber collimator used as the laser output coupler	9
4.	Mode beating spectra of the two component cavities and the compound cavity when one of the two component cavities has an additional 5 m of fiber inserted	10
5.	Mode beating spectra of a one-amplifier laser showing the polarization-resolved detection capability of generating spectra containing one or both orthogonal polarizations of the laser output	11
6.	Power spectra showing the longitudinal mode beating as the rotation of the polarization is changed	13
7.	Mode beating spectra without (bottom) and with (top) the fiber polarizer inserted	13
8.	Transmission spectra of the four FBGs that we have used in the experiments	15
9.	Schematic of the two-laser experimental configurations compared	17
10.	Optical spectra of the gratings and cavities for the Michaelson configuration	19
11.	Time characteristics of the Michaelson configuration cavities	19
12.	Optical spectra of the gratings and cavities for the Mach-Zehnder configuration	20
13.	Time characteristics of the Mach-Zehnder configuration cavities	20
14.	Schematic of the flexible experimental apparatus in a unidirectional ring configuration	22

15. Schematic of the amplifier segments for the multilaser configurations ..... 23 & 24

LIST OF FIGURES (continued)

Figure		Page
16.	Spectra generated by the output of the ring laser with the single 0.5-W amplifier	26
17.	Output power from a 2-laser baseline configuration with a 10-cm length mismatch between amplifier arms and when fiber is added to one arm to produce a 5-m length mismatch	28
18.	Power spectra when two of the four amplifiers are operating	29
19.	Output power as a function of measured pump level for the individual amplifiers in the two-amplifier configuration and when they are coherently combined	30
20.	The pulsation period of the two-laser system as a function of the pulse power	31
21.	Time trace of a series of pulsating data for two coupled lasers taken when amp 1:2 was pumped to the level 165.2 and the 500-mW amp was pumped at 111.1	32
22.	Upper plot – Relative output powers from each of the four constituent lasers when operated separately	34
23.	Output power from the 4-laser baseline configuration, dark blue curve, and when fiber is added to one arm	36
24.	Longer term output characteristics for the 4-laser configuration with 1 m of extra fiber in the amp 1:2 arm (dark blue curve) , and when this configuration is modified by adding 5 meters of fiber to the amp 2:1 arm	37
25.	Time trace of a long cavity, four-amplifier configuration	38
26.	Optical spectrum corresponding to the time trace in Figure 25	39
27.	Optical spectrum showing the changes due to a change in the smallest cavity length mismatch relative to Figure 26	40
28.	Power spectrum of the photodetected output of the laser array in the configuration corresponding to the optical spectrum in Figure 26	41

LIST OF FIGURES (continued)

Figure		Page
29.	Detail of the power spectrum of the photodetected output of the laser array in the configuration corresponding to the optical spectrum in Figure 26	42
30.	Detail of the power spectrum of the photodetected output of the laser array in the configuration corresponding to the optical spectrum in Figure 26	42
31.	Detail of the power spectrum of the photodetected output of the laser array in the configuration corresponding to the optical spectrum in Figure 26	43
32.	Schematic of a two-laser array configuration with an added coupler and fiber loop in one arm of the array	49

LIST OF TABLES

Table		Page
1.	Output power as a function of polarization enforcement and control	12
2.	Approximate cavity length to frequency conversions	35
3.	Relative output power in the four-laser configuration	44

ACKNOWLEDGEMENTS

The work and results described here have been undertaken with the ongoing collaboration of Drs. Phillip Peterson and Athanasios Gavrielides of the Air Force Research Laboratory. The author is indebted to them for their encouragement, support and continued willingness to dig into the details of this problem and search for the answers. Their parallel theoretical investigations have provided an underpinning for some of the experimental observations emphasized here. Also, the author gratefully acknowledges expert technical assistance with the experimental apparatus by Mr. Frank Doft of the Titan Corporation.

LIST OF ACRONYMS

DFB	distributed feedback
Er	Erbium
FBG	fiber Bragg grating
MSA	microwave spectrum analyzer
mW	milliwatts
RBW	resolution bandwidth
RF	radio frequency
SBS	stimulated Brillouin scattering

CONVERSION TABLE

Conversion factors for U.S. Customary to metric (SI) units of measurement.

MULTIPLY →	BY	→ TO GET
← TO GET	← BY	← DIVIDE

angstrom	1.000 000 × E −10	meter (m)
atmosphere (normal)	1.013 25 × E +2	kilo pascal (kPa)
bar	1.000 000 × E +2	kilo pascal (kPa)
barn	1.000 000 × E −28	meter^2 (m^2)
British thermal unit (thermochemical)	1.054 350 × E +3	joule (J)
calorie (thermochemical)	4.184 000	joule (J)
cal (thermochemical/cm^2)	4.184 000 × E −2	mega joule/m^2 (MJ/m^2)
curie	3.700 000 × E +1	*giga becquerel (GBq)
degree (angle)	1.745 329 × E −2	radiation (rad)
degree Fahrenheit	t_K = (t°f + 459.67)/1.8	degree kelvin (K)
electron volt	1.602 19 × E −19	joule (J)
erg	1.000 000 × E −7	joule (J)
erg/second	1.000 000 × E −7	watt (W)
foot	3.048 000 × E −1	meter (m)
foot-pound-force	1.355 818	joule (J)
gallon (U.S. liquid)	3.785 412 × E −3	meter^3 (m^3)
inch	2.540 000 × E −2	meter (m)
jerk	1.000 000 × E +9	joule (J)
joule/kilogram (J/kg) radiation dose absorbed)	1.000 000	Gray (Gy)
kilotons	4.183	terajoules
kip (1000 lbf)	4.448 222 × E +3	newton (N)
kip/inch^2 (ksi)	6.894 757 × E +3	kilo pascal (kPa)
ktap	1.000 000 × E +2	newton-second/m^2 (N-s/m^2)
micron	1.000 000 × E −6	meter (m)
mil	2.540 000 × E −5	meter (m)
mile (international)	1.609 344 x E +3	meter (m)
ounce	2.834 952 × E −2	kilogram (kg)
pound-force (lbs avoirdupois)	4.448 222	newton (N)
pound-force inch	1.129 848 × E −1	newton-meter (N-m)
pound-force/inch	1.751 268 × E +2	newton/meter (N/m)
pound-force/foot^2	4.788 026 × E −2	kilo pascal (kPa)
pound-force/inch^2 (psi)	6.894 757	kilo pascal (kPa)
pound-mass (lbm avoirdupois)	4.535 924 × E −1	kilogram (kg)
pound-mass-foot^2 (moment of inertia)	4.214 011 × E −2	kilogram-meter^2 (kg m^2)
pound-mass/foot^3	1.601 846 × E +1	kilogram/meter^3 (kg/m^3)
rad (radiation dose absorbed)	1.000 000 × E −2	**Gray (Gy)
roentgen	2.579 760 × E −4	coulomb/kilogram (C/kg)
shake	1.000 000 × E −8	second (s)
slug	1.459 390 × E +1	kilogram (kg)

torr (mm Hg, 0° C)	1.333 22 × E −1	kilo pascal (kPa)

* The becquerel (Bq) is the SI unit of radioactivity; 1 Bq = 1 event/s.

** The Gray (Gy) is the SI unit of absorbed radiation.

A more complete listing of conversions may be found in Metric Practice Guide E380-84, “American Society for testing and Materials.”

(This page intentionally left blank.)

SUMMARY

Experiments have been conducted to investigate the feasibility and scalability of coherent laser output from an array of fiber lasers with strong intracavity coupling. Previous work established that it was possible to achieve coherent output when the fiber lasers are mutually coupled through 2×2, 50/50 fiber couplers placed between the gain medium and the output coupler. Work by other groups has established that the coherent combining can be scaled to up to 8 lasers using a cascade of the 50/50 fiber couplers. In this investigation, we have concentrated on understanding the spectral characteristics of the coherent output.

A flexible, reconfigurable experimental apparatus that had been designed previously has been modified and configured for these investigations. The design has emphasized the use of commercially available components being developed for the telecommunications industry. The apparatus is built around five independent Erbium (Er)-doped fiber amplifiers and can be configured with optical isolators and an optical circulator to enforce unidirectional operation. A fiber Bragg grating (FBG) acts as a wavelength selective element in the cavity. Polarization selection and control for the intracavity fields is also provided. Measurements taken with this apparatus during this program showed that without polarization selection, the lasers were likely to exhibit spectra that showed the effects of polarization mode dispersion. Spectral features with frequencies and amplitudes that depended on intracavity polarization control were observed and could be eliminated through polarization selective elements.

Arrays of 2 to 5 amplifier elements coupled using the 2×2 fiber couplers were constructed with emphasis on a unidirectional ring configuration. Previous investigations of the two-amplifier configurations were extended. A theoretical prediction that for a range of pump powers more power can be coherently coupled out of an array than is available at all outputs of an incoherently coupled array was verified experimentally. Spectral features related to the mismatch in cavity length for the array elements were identified. A novel pulsating behavior was observed over a range of operating conditions for the two-element array. The pulsation

frequency was observed to increase with increasing pump power, at variance with the usual decrease in pulsation frequency.

An extensive series of runs was made where the overall cavity length or the lengths of individual element paths were varied over a wide range. Stable output from a four-laser array could only be observed when there was significant length mismatch between the array elements. Stable operation of a coherently coupled array appears to become increasingly difficult as the number of array elements is increased. We observed a transition in the spectral characteristics that indicated that cross coupling between optical modes was the first significant nonlinear optical interaction in the array, even though the power threshold for stimulated Brillouin scattering (SBS) is much lower. The spectra showed significant broadening in the nonlinear optical regime and under certain conditions could fill the range of high reflection of the FBG. However, relatively minor changes in cavity length or length mismatch could produce significant changes in the spectral characteristics.

The observations of novel pulsation behavior, spectral broadening and sensitive dependence of the spectra to small cavity changes indicate that the nonlinear optical interactions can play a significant role in the coupled array as the power is increased and the number of elements is increased. We observed that the nonlinear optical interactions sometimes, but not always, modified the spectra in a way that produced superior coherent output. There appears to be a complex interplay between the spectral broadening and the frequency selection that arises from length mismatches in the cavity. This complex interplay must be better understood in order to determine if the nonlinear optical interactions can be used to improve the output characteristics of the coherently coupled array that contains a large number of elements.

INTRODUCTION

There is considerable current interest in intracavity combining of fiber lasers to produce coherent output from multiple elements. This is motivated by the fact that individual fiber lasers will be limited to the kilowatt level[1] and some applications, such as coherent scene illumination for imaging and laser-radar applications, particularly for space-based systems, require orders of magnitude higher power levels. Achieving considerably higher power in a coherent beam will require the coherent combining of the output from several fiber lasers or amplifiers. A variety of techniques can be used to generate coherent beams from multiple sources. This report describes a particularly simple configuration, based on the use of commercially available 2 × 2, 50/50 fiber couplers. Previous work had shown that coherent coupling was possible using a cleaved, 2 × 2 fiber coupler, where the cleaved facet in the coupler interaction region was used as the common output coupler.[2] We then demonstrated that it was not necessary to use a specially designed, cleaved coupler but that mutually coupled lasers would "self-organize" to produce coherent output if this reduced intracavity losses and maximized circulating power.[3] A two-laser cavity such as that shown in Figure 1 would spontaneously configure the output so that the power that emerged from the loss port D of the 2 × 2 coupler was minimized while that transmitted through the output coupler B, and, therefore, also fed back into the cavity, was maximized. Subsequently, Sabourdy, et al., reported a similar configuration using a Mach-Zehnder type layout.[4]

These configurations are appealing because they are simple to construct with commercially available components and are readily augmented to include additional lasers by cascading multiple 2 × 2 couplers in tree configurations. However, while subsequent reports have demonstrated four[5,6] and then eight lasers[7] coupled in this way, it quickly became clear that the configuration could not scale too many lasers easily. This was the due to the effects of unavoidable length mismatches between the different fiber arms of the array. It was demonstrated that if two different lasers could not be stabilized and matched in length to within a wavelength that a minimum length mismatch was necessary to insure coherent

output. The minimum

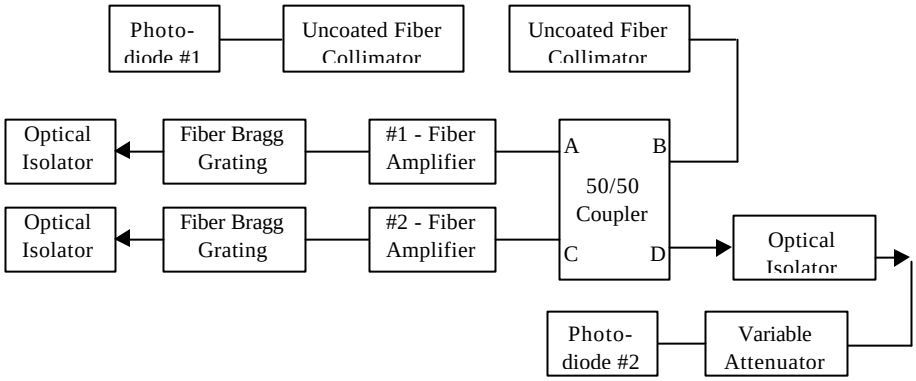

Figure 1. Schematic of the basic two-element configuration that demonstrated self-selected coherent output. The elements of the coupled cavity are highlighted in blue. Optical isolators are used to prevent backscattering of light into the cavity. Polarization matching was achieved by twisting and clamping a fiber pigtail in one arm of the cavity.

mismatch is closely related to the high-reflection bandwidth of the FBGs used as cavity rear reflectors due to the interferrometric nature of the laser cavity.[4] A statistical model of laser mode overlap reproduced the coherence properties of the configuration as the array was scaled up to eight lasers.[7] While the fractional power coherently coupled out of the laser was still high with an eight-element array, the trend clearly indicated that coherence would rapidly drop with additional elements.[7]

In this work we investigate whether one could use nonlinear optical effects within optical fibers to assist the self-organization process and maximize the coherent output. Previously, the fiber lasers used in these studies have been relatively short, ~10 to 20 meters (m), and low power, on the order of 100 milliwatts (mW) per array element. Here we report investigations of long cavities, up to ~800 m, where nonlinear optical effects could be observed. While the relatively narrow-band SBS has the lowest threshold of the nonlinear optical processes in fibers, we observed that it was much weaker cross modulation effects due to the background

broadband nonlinearity that produced the strongest changes in the optical output characteristics.

We modified and used a flexible experimental apparatus originally constructed in an earlier program[8] to investigate the nonlinear optical interactions. Our principal method for investigating details of the output was to measure the output spectrum, both the optical spectrum and the photodetector power spectrum. Early on in the investigation, we observed spectral effects due to the fact that a standard single-mode fiber has two nearly degenerate orthogonally polarized modes. In the next section, we review some features of the experimental apparatus and the polarization results that we observed. We also present some results comparing two linear cavity configurations, a Michaelson-type coupled cavity and a Mach-Zehnder type. These results caused us to reconfigure the apparatus with an intracavity fiber polarizer and reconfigure the lasers in a ring configuration. Details of this reconfiguration are given. Following this, results using a two-laser ring cavity are presented and then the results on investigations of four- and five-laser arrays. Here we observed stable operation with relatively short lasers and significant length mismatches, and significant broadening of the spectra when nonlinear interactions play a role in long cavities. We also describe results that imply a high sensitivity of the optical output to small changes in the lengths of the laser cavities of multi-element arrays. Finally, conclusions are summarized and recommendations given.

POLARIZATION - RESOLVED MEASUREMENTS AND LINEAR-CAVITY COMPARISONS

The experimental apparatus was constructed with attention to two key goals. First, it was to be flexible to allow a variety of cavity implementations to be configured and easily reconfigured. Second, to the greatest extent possible, it was built using commercially available components to minimize cost and maximize flexibility, ease of use, and the ability to incorporate design changes as the program progressed. Throughout, the apparatus design emphasized the use of cost-effective, commercially available fiber components being developed for the telecommunications industry. The array is designed around Er-doped fibers as the amplifying medium. Er-doped fiber amplifiers are now available from a variety of vendors. Most units, however, are focused on the telecommunications market and do not emphasize high powers. Because high power applications are of significant interest to the Air Force, we were interested in fiber gain media that could be scaled to high power levels. Dual-cladding or cladding-pumped fibers have been used almost exclusively in the fiber laser systems that have achieved the highest power levels. Therefore, we were interested in using these fibers as the gain media for the array. Each element is under independent gain control and is individually connectorized for coupling to additional optical elements. There is no internal crosstalk between elements of the amplifier array so that all coupling is under external control. FBGs with a high reflectance (>99%) bandwidth of ~50 GHz were used to select the output wavelength range. The use of connectorized optical fiber components allows ready reconfiguration of the array. All connectors for the array are of the FC/APC type. These connectors introduce very small loss, <0.5 dB, and minimal reflections, <60 dB, in the optical cavity. Minimizing unwanted reflections is essential for control of the coupling between the individual cavities of the fiber laser array. Details of the hardware are given in Reference 8.

At the beginning of the current program several changes were made to improve the ability to monitor polarization effects. We initially concentrated on the two-laser configuration shown in Figure 1 and added polarization control to each of the component laser cavities. The

commercial components, from Newport, rotate the polarization by applying stress to a fiber in a more precise way than the simple twisting and clamping of the fiber that we originally used. They add a short length of fiber so that the basic cavity frequency drops from about 6 GHz to about 5.8 GHz. Further; we modified the cavities by adding lengths of fiber. Between the fiber amplifier and the FBG there is approximately 2 m of fiber pigtail and an FC/APC connector. Connectorized fiber patchchords of 1 m, 5 m, 30 m and 200 m were purchased and could be easily inserted and removed at the connector. The base length of each of the component lasers is approximately 16 m. Therefore we could implement a wide range of cavity ratios and/or extensions. The longest length patchchord was expected to be sufficient to ensure that SBS will occur in the region between the amplifiers and the FBG. A schematic of the modified cavity is shown in Figure 2.

We also configured an improved polarization-resolved detection scheme shown schematically in Figure 3. With this configuration of elements outside of the laser we could observe the total laser output and simultaneously resolve two orthogonal polarizations. The photodiode signals were monitored with oscilloscopes and a radio frequency (RF)/microwave spectrum analyzer (MSA) to get the complementary temporal and spectral information. The addition of optical isolators prevented feedback from the uncoated fiber collimators from reaching the laser cavity.

Theoretical work by A. Gavrielides and P. Peterson predicted that the compound laser cavity would oscillate on a set of modes that were distinct from the modes of the component laser cavities but that the modes with overlapping frequencies would show the highest output power.[9] By inserting the extra lengths of fiber into the laser cavity we could control the mode frequency of the longitudinal modes. The compound laser cavity showed the predicted characteristics. Figure 4 shows a power spectrum of the polarization-resolved output from the laser cavity when an extra 5 meters of optical fiber was added to one of the two component laser cavities. The polarization of the laser output had been rotated with the $\lambda/2$ plate in Figure 3 so that the polarization would be aligned with the axes of the beamsplitter cube. The

frequency separation of the laser modes is about 5.8 MHz in the shorter component laser cavity and 4.4 MHz in the longer cavity. To generate the spectrum the RF/MSA was set to its "peak hold" setting. In this

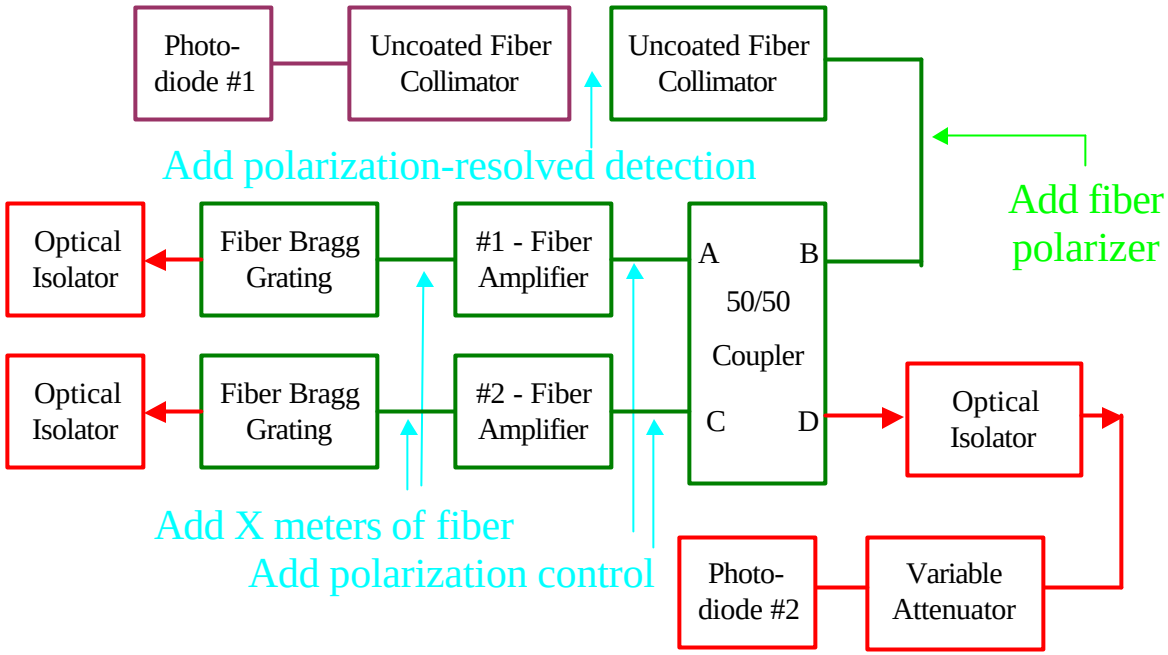

Figure 2. Schematic of the two-laser configuration with the modifications that have been implemented to study issues related to polarization of the optical output and cavity length mismatch. The components marked in green are the basic compound linear cavity configuration. Those parked in purple are the output detection elements and in red are elements at the loss ports that prevent feedback and allow monitoring of the coherence. Modifications/reconfigurations to the apparatus that were made in the current program are noted.

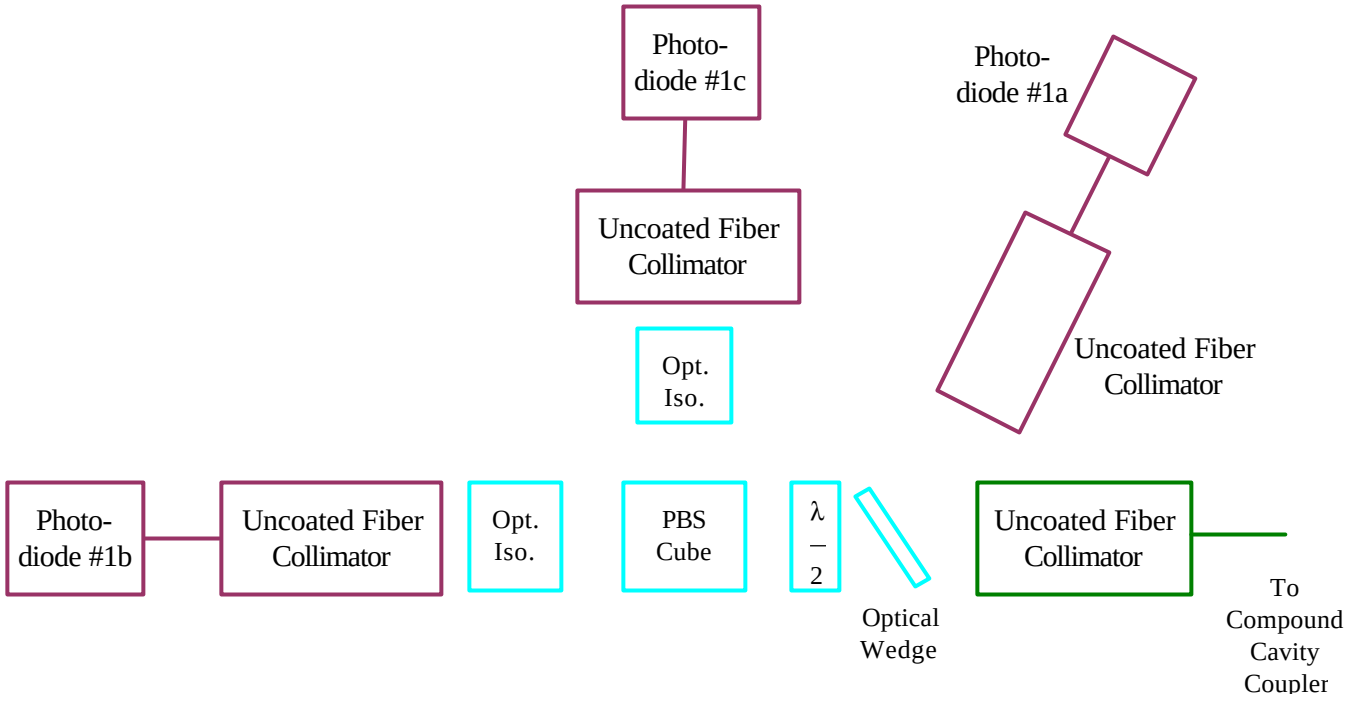

Figure 3. Schematic of the optical path outside of the fiber collimator used as the laser output coupler. Photodiode #1a monitors the total output power while photodiodes #1b and #1c monitor orthogonal polarizations. The l/2 plate rotates the laser output polarization and the optical isolators prevent feedback into the laser cavity.

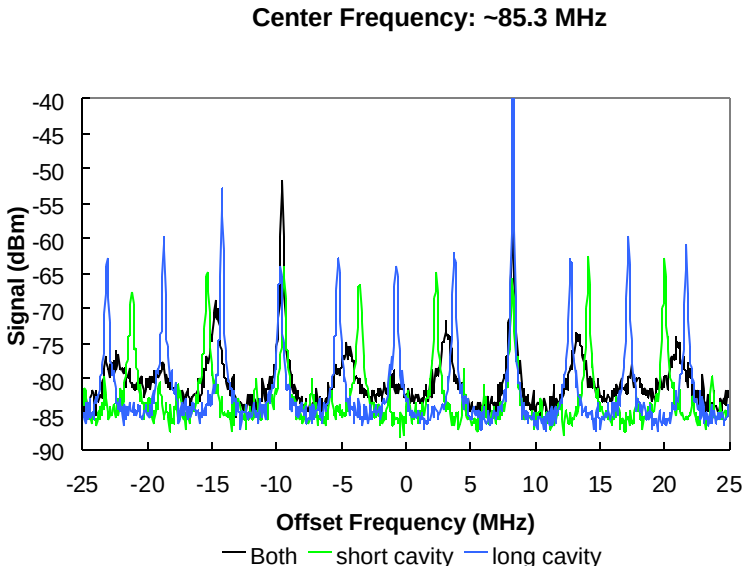

Figure 4. Mode beating spectra of the two component cavities and the compound cavity when one of the two component cavities has an additional 5 m of fiber inserted.

setting, the highest power reading in each frequency bin is saved during sequential scans. Because the laser is randomly oscillating on different optical modes, the beating of particular modes occurs randomly. This technique allows all the strong modes to be displayed. The spectra show that the mode frequencies of the compound cavity are distinct from the two component cavities, in agreement with the theory, and that significant power only appears in those modes that are simultaneously nearly resonant with the modes of the component cavities, again in agreement with theory. Good coherence was maintained when the length of one of the two cavities was different, even by as much as 200 m of fiber.

With the polarization-resolved detection apparatus we could clearly see evidence of the orthogonal polarizations. As an example, Figure 5 shows the situation when only one amplifier is operating. Using the $\lambda/2$ plate shown in Figure 3, we rotated the output polarization of the lasers. The "one polarization" trace shows the output when the two laser polarizations are aligned with the polarizing beamsplitter so that only one polarization component reaches

detector 1b or 1c.

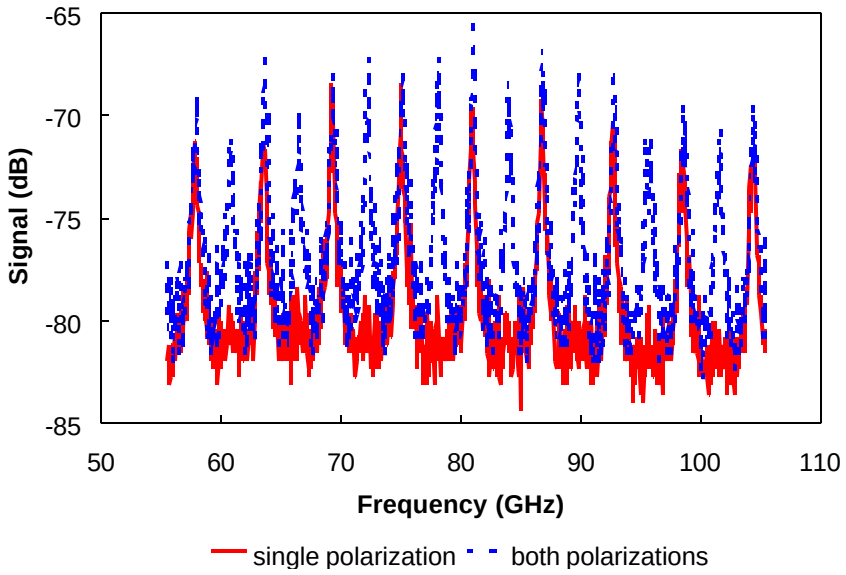

Figure 5. Mode beating spectra of a one-amplifier laser showing the polarization-resolved detection capability of generating spectra containing one or both orthogonal polarizations of the laser output.

When the λ/2 plate is rotated so that both polarizations are passed to both detectors then the "two polarization trace" is observed. Note that twice as many modes appear due to the beating between the orthogonally polarized modes. Normally these modes would not produce a beat signal at the detector but the polarizing beamsplitter cube transforms the beam polarization characteristics of the transmitted beam. There is some evidence of weak orthogonal polarization mode beating in Figure 4, particularly for the short cavity spectrum. In this case, however, the beat frequencies are about 1/3rd and 2/3rd between the dominant peak. The polarization mode dispersion appears to depend on the details of the particular cavity involved.

To eliminate the complicating feature of the orthogonally polarized modes, we added a fiber polarizer to the cavity common-path leg as shown in Figure 2. This polarizer enforced a unique polarization direction for the circulating laser field, suppressing the two-polarization output that we had observed previously. In addition to the polarization selection, the polarizer, and the two meters of fiber pigtail, changed the cavity length. It also caused some change in the output power as summarized in Table 1. The table summarizes the changes to the output when one of the two fiber amplifiers is pumped and the other is left unpumped. The laser output power is compared for three cavity configurations at different pump levels. In the No Polarizer and Rotator configuration all polarization enforcement and control components are removed from the laser cavity. After this the polarizer is inserted into the laser cavity and then, finally, the Rotators are added to the laser cavity. Adding the polarizer reduces the laser output power. However, the loss is more then compensated when the polarization rotators are added and adjusted to maximize the output power.

Table 1. Output power as a function of polarization enforcement and control.

Pump Power (arb. units)	**Output Power (arb. units)**		
	No Polarizer & Rotator	**Polarizer/No Rotator**	**Polarizer & Rotator**
72	threshold	threshold	threshold
86	222	165	216
104	575	480	638
123	970	830	1110

The effects of the polarization on the power, or longitudinal mode beating, spectra are shown in Figures 6 and 7. In Figure 6 the laser is configured with the polarization rotators but without the fiber polarizer. Again, only one amplifier is pumped. The different spectra show changes as the rotation induced by the polarization rotators is changed. The detection apparatus at the

laser output is configured so that the two orthogonal polarizations can beat together at the detector by selecting a polarization direction that is not parallel to either of the polarization axes of the output field. The beating of each polarization component with itself produces the strong spectral components offset by approximately 5.8 MHz. The weak peaks are produced by the beating of orthogonal components. The polarization rotator changes the frequency offset between the two frequency combs of the orthogonal polarizations as it rotates the polarization. This is shown by

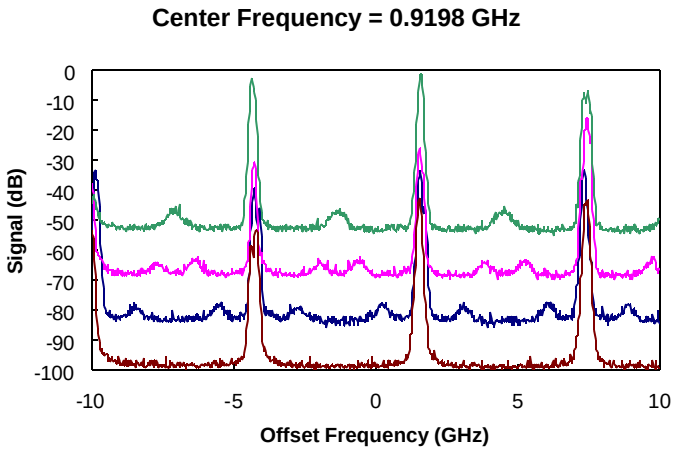

Figure 6. Power spectra showing the longitudinal mode beating as the rotation of the polarization is changed. The strong peaks spaced by approximately 5.8 MHz are due to the beating of longitudinal modes within each polarization component. The weak peaks in between result from beating of orthogonal polarization components. The polarization rotators change the intracavity polarization mode dispersion, shifting the optical frequencies of the different polarization components. The spectra are offset vertically as an aide for viewing only.

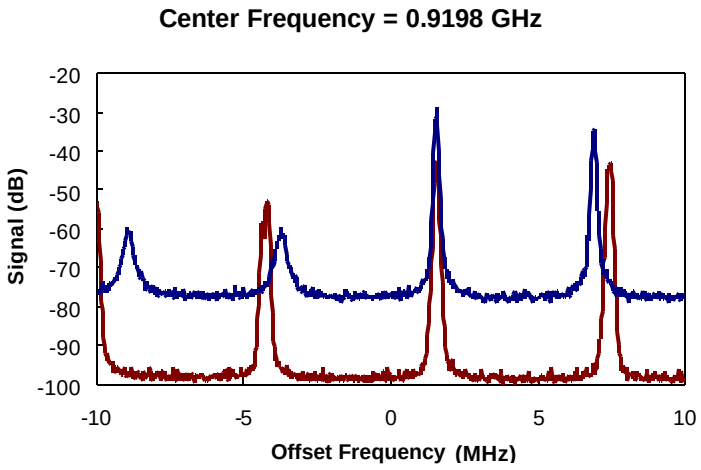

Figure 7. Mode beating spectra without (bottom) and with (top) the fiber polarizer inserted. The bottom curve is a repeat of the bottom curve from Figure 2 where the polarization rotator was adjusted so that the weak orthogonal polarization beating peaks are degenerate with the strong peaks. With the polarizer, there are no weak peaks for any adjustment of the rotators. The mode beating frequencies are shifted when the polarizer is inserted due to the addition length of the polarizer and fiber pigtails.

the shift of the offset frequency of the weak peaks. The rotators can even shift the offset frequency so that these features disappear, as shown in the lowest trace. When the polarization rotator is added, there are no weak features between the main components, as shown in Figure 7, where the output with the polarizer is compared to the case without the polarizer but with the rotators adjusted so that there are no weak beat components to the spectrum. The mode beating frequencies are shifted when the fiber polarizer is inserted due to the increased cavity length. With the polarizer, however, there are no weak components for any adjustment of the polarization rotators. In this way, we could eliminate the complicating artifacts of the orthogonal fiber polarizations from our subsequent spectra without reducing the circulating power level.

The theoretical work by Gavrielides and Peterson also predicted that the ratio of the output power from the compound laser cavity shown in Figure 2 could be more than four times the output of a component laser cavity biased to the same level when the other laser was off.[9]

This could occur near threshold. We checked this and found that this was indeed true. The value of four is an asymptotic value as the pumping level is increased above threshold, as predicted by the theory. We observed that this value was reached, to within a 10% experimental accuracy, at bias levels of 33% above threshold. Our previous data had been taken at bias levels of approximately 50% above threshold, or higher, so that this feature had not been observed.

After we had made these measurements, we became aware that groups at HRL in Malibu, CA, France and Japan had all achieved stable operation of four-element arrays. At this time, we had been unable to produce stable coherent output with more than two elements. The lasers would spontaneously switch between stable output and power oscillations at frequencies consistent with the relaxation oscillation frequency. We suspected that we were being limited by parasitic reflections that corrupted the cavity or by anomalies in our FBGs. However, the French group used a somewhat different configuration, based on the Mach-Zehnder interferometer.[4,6] We also wanted to compare configurations.

We looked at the spectral characteristics of our FBGs. Figure 8 shows the transmission characteristics as a DFB laser diode is scanned in optical frequency across the stop band of the gratings. The gratings are used as high reflectors so that the overlap of the transmission stop bands is the relevant parameter. Previously, we have been unable to take spectra across the entire grating in a short time because we have only had the capability to wavelength tune the DFB laser diode by changing its operating current. To overcome this, we purchased a temperature controller that allows analog control of the temperature. We have observed that the laser diode follows temperature changes over the required range on a time scale of a few seconds. The four gratings are labeled by their center wavelengths in nanometers as specified by the manufacturer. An offset of 0.1 nm corresponds to a frequency shift of approximately 12.4 GHz at these wavelengths. As can be seen, the offset of the high and low frequency gratings is significantly larger than originally measured, sufficiently large so that there is only poor overlap between the two gratings. If this poor overlap existed at the time of our earlier measurements of the four-laser array, then this could explain the relatively poor performance characteristics that we observed.

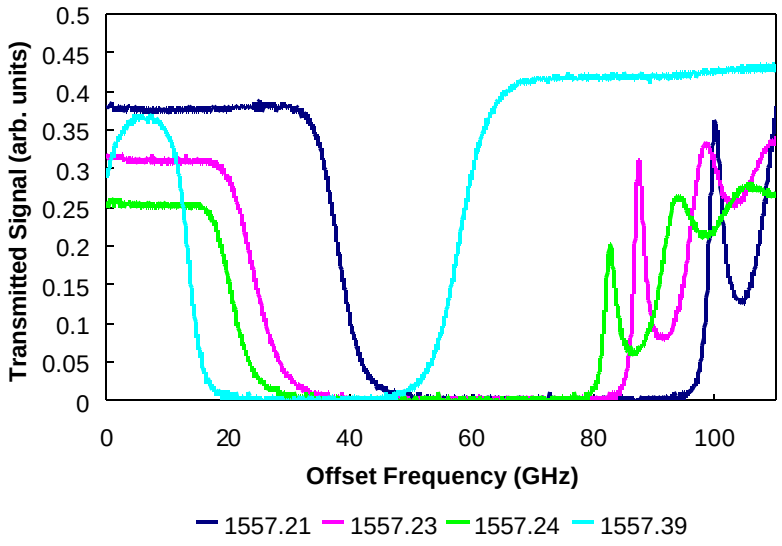

Figure 8. Transmission spectra of the four FBGs that we have used in the experiments. The gratings are labeled by the center wavelength as specified by the manufacturer. An offset of 0.1-nm corresponds to an optical frequency shift of approximately 12.4 GHz.

If a grating has become stretched, its center wavelength will shift to longer wavelengths. This might explain the mechanism for the wavelength shift. In the measurements reported below that use two gratings, we used the two gratings that displayed the best overlap, labeled 1557.23 and 1557.24.

We initially concentrated on two-laser configurations and compared performance in our standard, or so-called Michaelson or Fox-Smith, configuration and the Mach-Zehnder configuration. The layouts of the two are compared in Figure 9. They differ only at the high reflector ends of the cavities where the former uses one grating for each cavity while the latter uses a second 50/50 fiber coupler to combine the beams to a single grating for feedback. One (or two) fiber polarization rotators could be inserted between the amplifier(s) and the common 50/50 coupler. Detectors were positioned at loss ports as well as the output port to monitor the temporal and spectral properties and the coherence. In a later section, we will describe a unidirectional ring configuration that was investigated more extensively.

At this time. we also became concerned about the possibility that weak scattering or reflections off of the fiber connectors was corrupting our data by creating unwanted intracavity etalons. We purchased a fiber inspection microscope so that we could easily inspect the fiber connectors and observed that the fiber ends showed some build-up of dirt. A commercial fiber cleaner was sufficient to get the surface quality back in most cases. However, some imperfections are more difficult to eliminate. We also purchased a polishing puck that allows us to re-polish the angled FC/APC connector surface when that is necessary. To date, this has usually been sufficient to clean the end surfaces of our FC/APC connectors, though, as we discuss further at the end of this report we have not been able to isolate the source of all of the etalon-like effects.

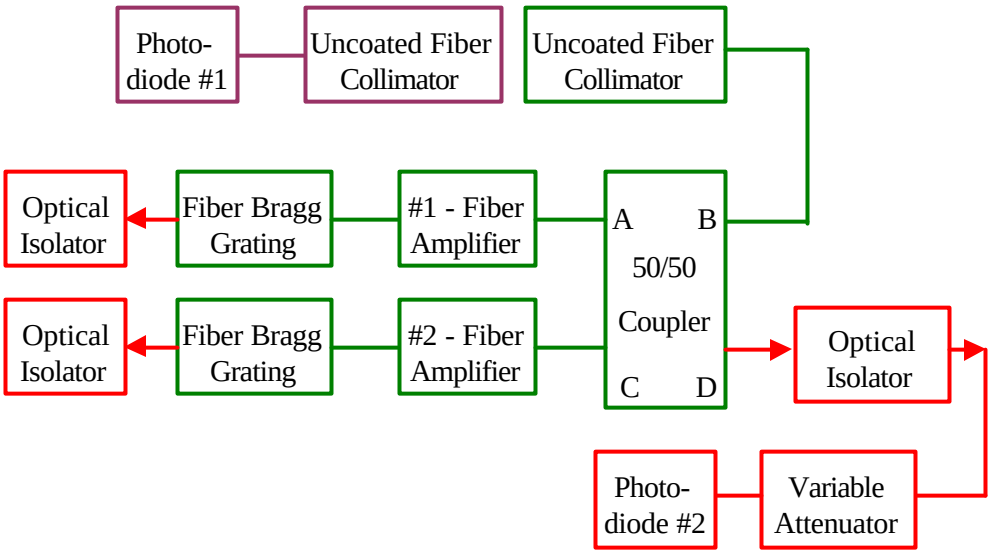

Figure 9(a). Michaelson configuration.

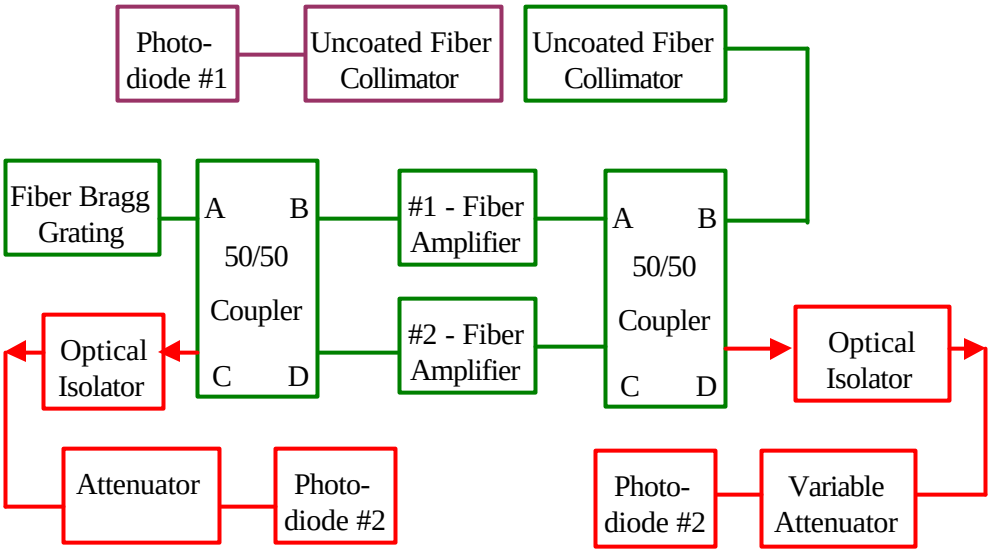

Figure 9(b). Mach-Zehnder configuration.

Figure 9. Schematic of the two-laser experimental configurations compared. The Michaelson configuration, Figure 9(a) is the base configuration that we have used previously. The Mach-Zehnder configuration, Figure 9(b) has been used by the French group. [4,6]

We generated some optical spectra, and corresponding temporal traces of output power, to compare the Michaelson and Mach-Zehnder configurations. Figures 10 and 12 compare the spectra of the Michaelson and Mach-Zehnder, respectively, while Figures 11 and 13 compare the slow time response. Note that in Figure 12, the optical spectra for the solitary cavity is a repeat of the data from Figure 10 in the Michaelson configuration with one amp unpumped. The Mach-Zehnder cavity actually has more loss, but the solitary cavities had qualitatively similar temporal characteristics. For the optical spectra, a key difference is that the nearly matched cavity length coupled cavities contain only one or two clusters of modes while the mismatched cavity length coupled cavity and the solitary cavities contain on the order of 10 mode clusters. By measuring the offset of high order modes of the power spectrum, we were able to determine the small length mismatch in the case of nearly matched cavities. There was a 100-kHz offset for the modes separated by approximately 933 MHz, corresponding to a length mismatch of about one part in 10^4, or 1-2 mm. With this small length difference only one or two modes simultaneously resonant with both cavities can be expected within the stopband of the grating. Mechanical fluctuations are likely to make this mode more or less ideal due to random perturbations, including polarization perturbations, and this is a potential explanation for the greater jitter in the laser output power for the nearly matched cavities. We will discuss this further in the section on two-element ring cavity measurements. The other point of comparison is the relative stability of the different coupled cavity configurations. Note that the Mach-Zehnder cavity, with its two points of loss controlled by coherence, is likely to have a greater sensitivity to polarization changes in the cavity. This cavity shows less stability but both cavities are not free from fluctuations on short time scales. The Mach-Zehnder also shows long time variations in the output that are stronger than the Michaelson case.

Eventually, we were able to generate stable output with four-laser Michaelson and Mach-Zehnder configurations. However, we always found that there appeared to be a high sensitivity to environmental changes with these configurations, particularly the Mach-Zehnder one. Therefore, soon after generating the data above, we decided to concentrate on a ring laser configuration. Other groups are investigating both the Michaelson and Mach-Zehnder linear configurations,[6,7] and it is not clear that we have any additional insight to add

to their published contributions. Further, there is a better hope of modeling the ring configuration, and this is underway at AFRL. Therefore, we terminated our work with the linear configuration and used the flexible nature of our apparatus to reconfigure to a unidirectional ring configuration. This work will be described next.

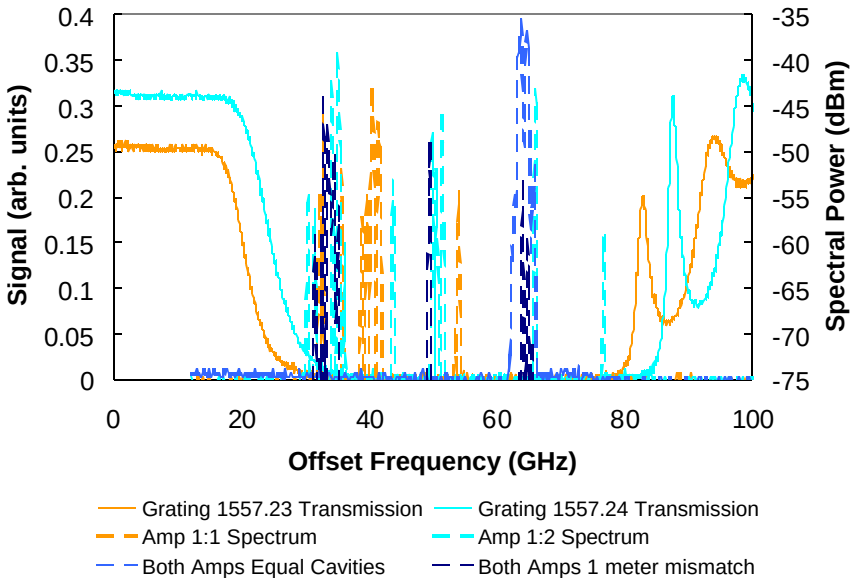

Figure 10. Optical spectra of the gratings and cavities for the Michaelson configuration. The optical frequency is taken with respect to an arbitrary, but identical, frequency for the four scans.

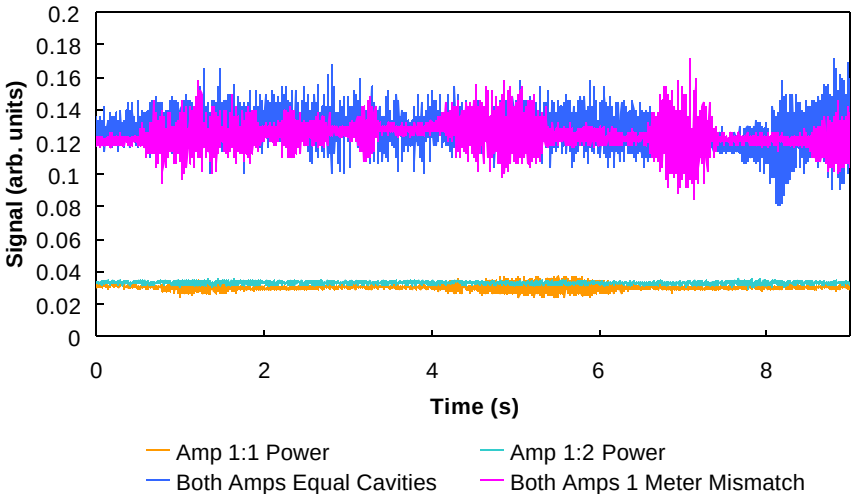

Figure 11. Time characteristics of the Michaelson configuration cavities.

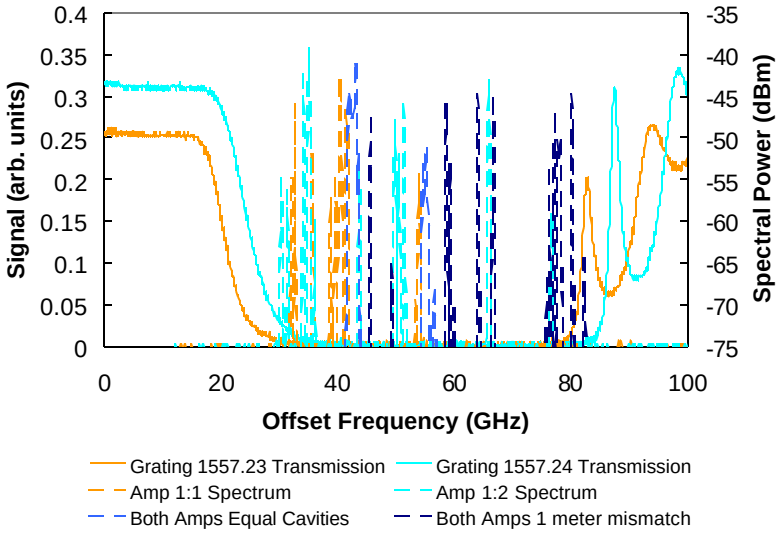

Figure 12. Optical spectra of the gratings and cavities for the Mach-Zehnder configuration. The optical frequency is taken with respect to an arbitrary, but identical, frequency for the four scans. Only the 1557.24 grating was used.

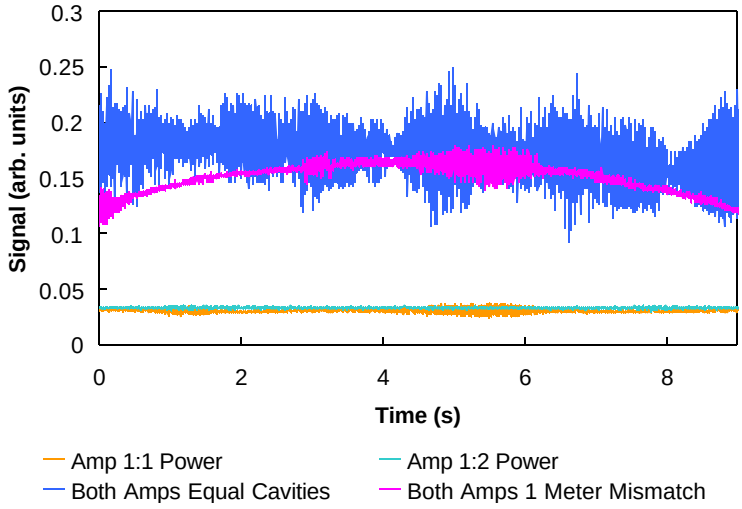

Figure 13. Time characteristics of the Mach-Zehnder configuration cavities.

RING-LASER RECONFIGURATIONS

For the investigations of a unidirectional ring-laser cavity, provision was made for arrays of from 2 to 5 amplifier elements. A fifth amplifier that is higher power, 500 mW instead of 100 mW, so that it can more than double the overall array output, has augmented the four amplifier elements originally used.[8] Figures 14 and 15 are schematics of the ring laser configuration built around the independent Er-doped fiber amplifiers. Figure 14 shows a single amplifier configuration that highlights the common loop components of the ring configuration and the diagnostics. The laser power circulates clockwise in the ring due to the directional character of the intracavity optical circulator and optical isolator. The fiber polarizer forces oscillation on one polarization axis only and the polarization rotator compensates for any polarization rotation in the ring. The FBG defines a narrow spectral band, typically ~30 to 50 GHz with our units, where the cavity round trip losses are minimized. Extra lengths of fiber can be added in different sections of the ring. Because there is about 5-dB loss through the optical circulator, adding the fiber after the circulator rather than before puts a lower intensity beam through any extra fiber in the common path. Adding between the FBG and the circulator causes twice the path length change for a given length of fiber plus the fact that there is now the potential for nonlinear interaction of the counter-propagating beams in a long segment. We increased the cavity length by up to 400 m of fiber, an 800-m path length change when the extra fiber is added between the FBG and the circulator. Light is coupled out of the ring at a fiber coupler. We typically use 10% output coupling though 50% and 90% are readily accommodated. The output light is directed to photodiodes whose temporal output is monitored using oscilloscopes and spectral output is monitored with a MSA. The output can also be mixed with a single-frequency distributed feedback (DFB) semiconductor laser that is used as an optical local oscillator to generate optical spectra. The temperature of the DFB laser is varied so that its frequency is swept across the high-reflection band of the FBG. A sweep takes about 10 seconds so that second and sub-second fluctuations in the optical spectra cannot be followed.

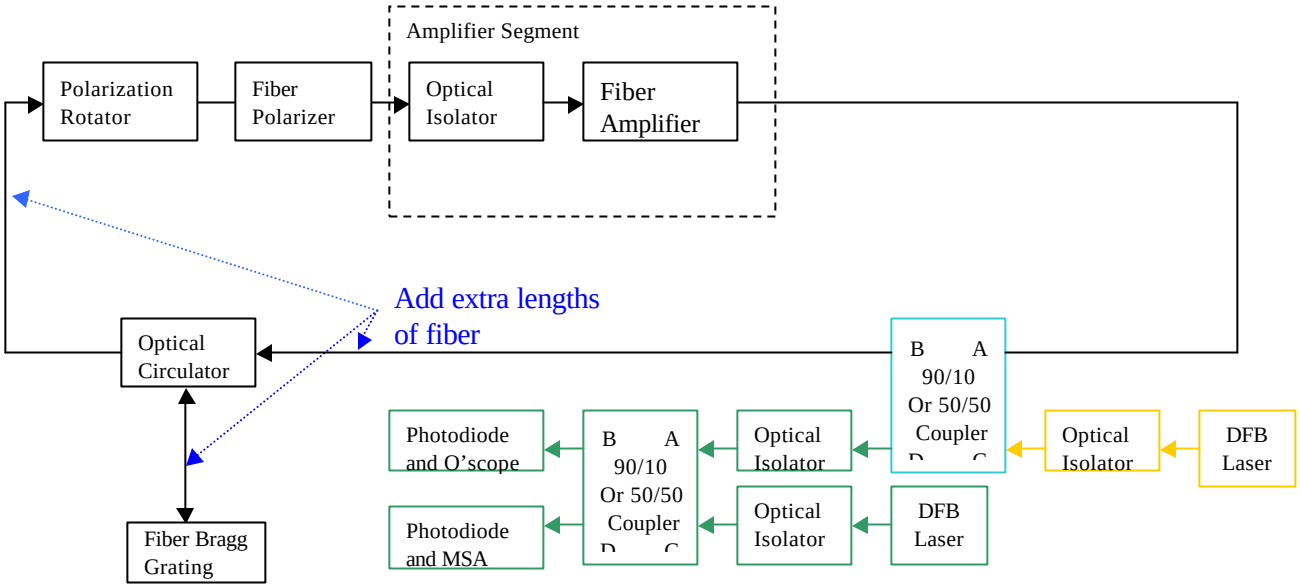

Figure 14. Schematic of the flexible experimental apparatus in a unidirectional ring configuration. Shown here is the configuration with a single amplifier. The 90/10 or 50/50 coupler with the light blue outline is the cavity output coupler. The elements outlined in green are the output diagnostics path with the DFB laser here used as a local oscillator to generate optical spectra with the photodiode and MSA. The other DFB laser is used to inject a single frequency optical signal into the cavity. Extra lengths of single mode fiber can be added to the cavity. The difference between adding the extra fiber before or after the optical circulator is the reduced circulating power after the circulator. Adding the fiber between the circulator and the FBG doubles the optical path for a given fiber length and adds the path where there are counter propagating beams. The optical circulator and the optical isolators enforce unidirectional optical beam circulation within the cavity.

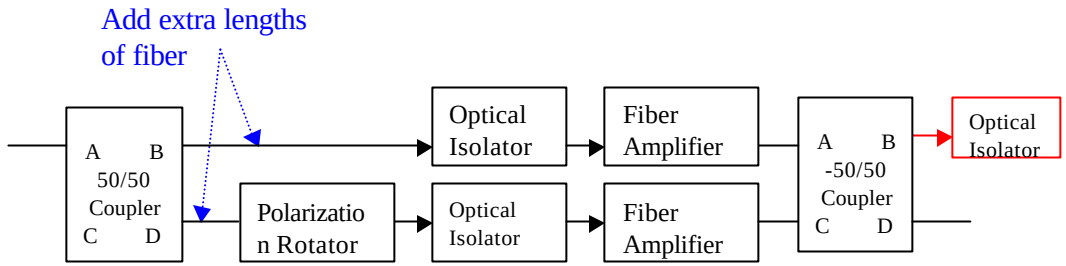

Figure 15(a). Schematic of the two-amplifier segment.

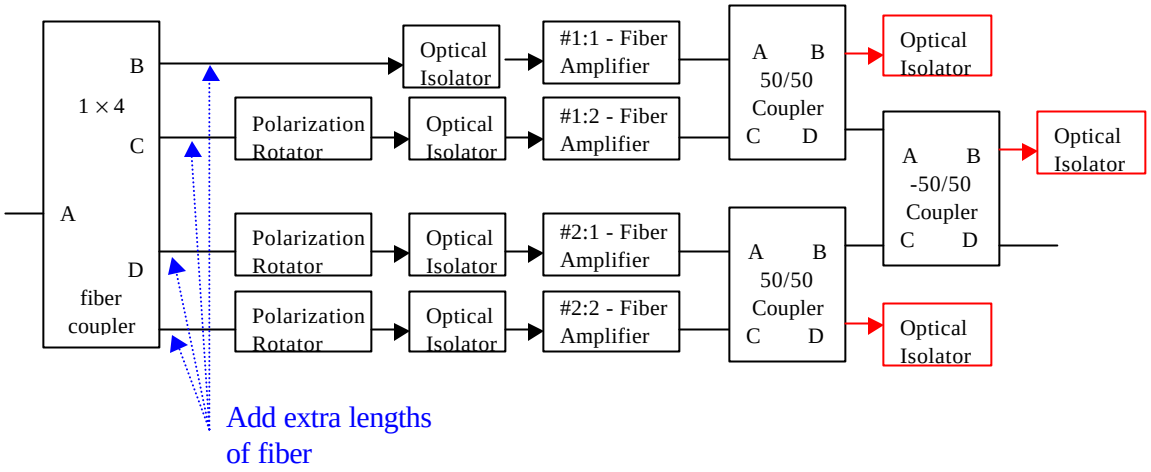

Figure 15(b). Schematic of the four-amplifier segment.

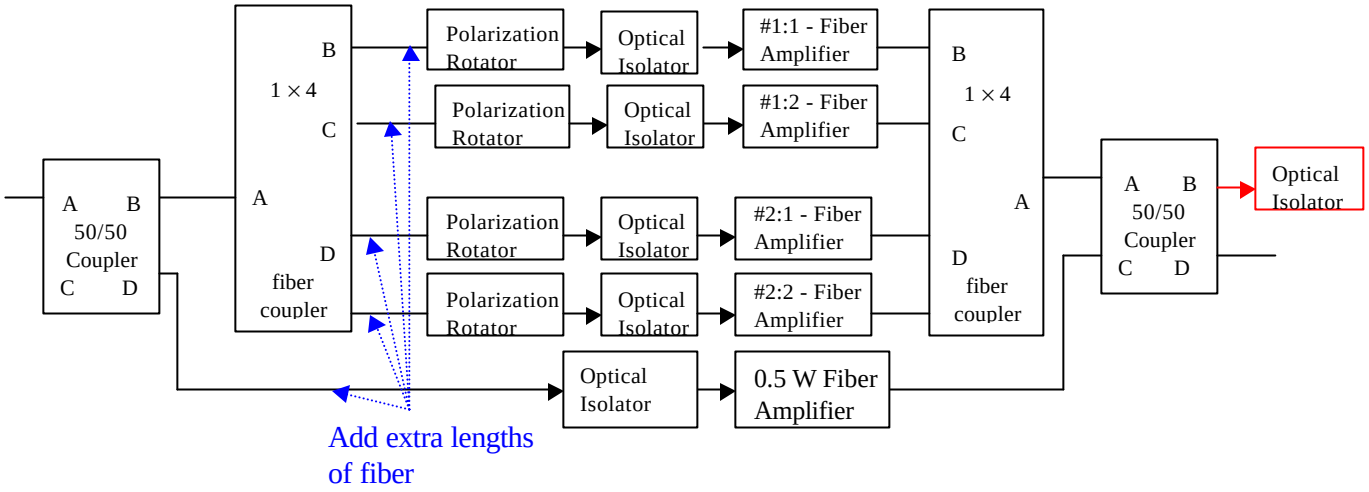

Figure 15(c). Schematic of the five-amplifier segment.

Figure 15. Schematic of the amplifier segments for the multilaser configurations. The optical isolators marked in red at the outputs of the 2 (a), 4 (b), and 5 (c) amplifier segments are the loss ports minimized by coherence that can be monitored with photodetectors. The empty input port c of the input 50/50 coupler in configurations (a) and (c) is typically configured with a 20-dB optical attenuator to effectively eliminate backscattered light. The input and output lines fit into the connections at the edges of the dashed box labeled Amplifier Segment in Figure 1. Extra lengths of fiber can be added to vary the length mismatch in the various arms of the array.

Scaling to more than one amplifier is accomplished within the box marked Amplifier Segment in Figure 14 and shown schematically in Figure 15. The two-amplifier configuration, Figure 15(a) uses 50/50 fiber couplers to split and remix the optical beams. A second polarization rotator is needed in one leg to correct for the fact that each amplifier may induce a different polarization shift. Alternatively, moving the rotator from the common path segment to the amplifier arm to match the components in the two arms creates a more symmetric configuration. Extra fiber can be added in either arm to vary the length mismatch. We used patchchords of 1 m and multiples, with some shorter length path variation possible with the repositioning of the fiber polarizers, i.e., moving the polarization rotator in the common leg to the amplifier arm that contains no rotator. Similar considerations apply for the four-amplifier configuration shown in Figure 15(b). The five-amplifier configuration, Figure 15(c), makes use of the fact that we have four 100 mW and one 500-mW Er-doped fiber amplifiers. The single larger amplifier can match the combined output of the four smaller ones. The 2×2 coupler (chains) contain output ports that can be monitored to observe the coherent combining. When coherence is maximized output at these points is minimized.

We first tested the new 500-mW amplifier in the single-amplifier configuration using both relatively short, ~25-m fiber length, and long, 425-m fiber cavities. As with the lower power amplifiers, power scaled linearly with pump level above threshold. Significant in the long cavity configuration was a broadening of the optical spectrum as the input power was increased. Figure 16 shows the broadening of both the optical, Figure 16(a), and power, Figure 16(b), spectra with increased power. Such broadening was not observed in the shorter cavity configuration. This broadening is indicative of a nonlinear optical effect where both optical power and interaction pathlength play a role in generating the signal. Significant broadening is observed at circulating power levels on the order of 30 mW (equivalent to the Power = 100 level in Figure 3) in cavities of approximately 400 m. Using a canonical value of 1/(W·km) for the fiber nonlinear coupling coefficient,[10] one observes the broadening when the cross-mode coupling is on the order of 1%. At this level, one observes a transition to an optical spectra with broadened, features with a relatively slow or smooth variation from mode to mode. There is some broadening at lower power levels but it tends to be highly structured and temporally varying. We believe that this lower power broadening relates to cavity imperfections, like parasitic intracavity reflections. For the shorter cavities, these power levels tend to exhibit a pulsating output at the relaxation resonance frequency. For all the amplifiers, there was a

range of pump levels where the laser displayed the pulsating output. The range varied from quite narrow, a few percent of the threshold value, to a range from just above threshold to approximately twice threshold.

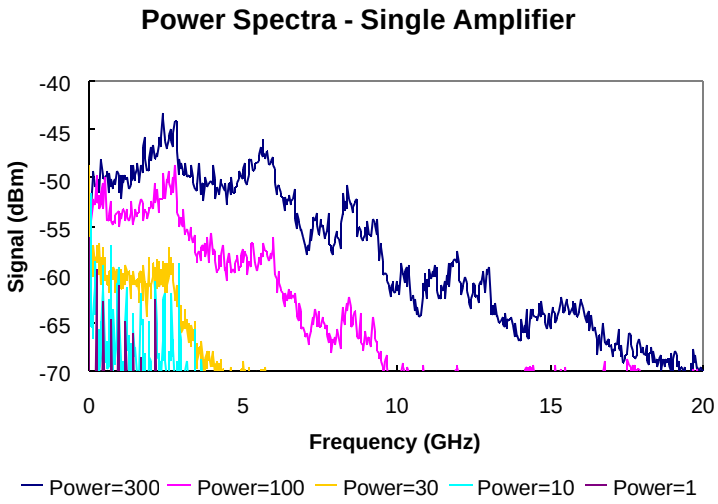

Figure 16(a). Long cavity single amplifier – Optical spectra.

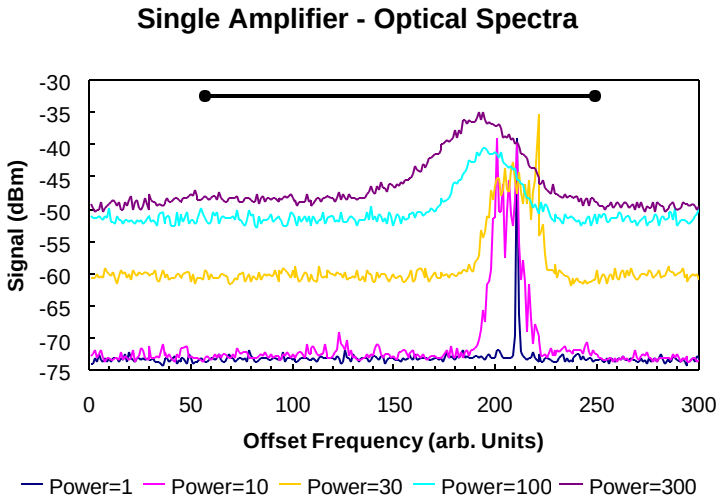

Figure 16(b). Long cavity Single amplifier – Power Spectra.

Figure 16. Spectra generated by the output of the ring laser with the single 0.5-W amplifier. (a) Optical spectra and (b) power spectra at a range of different power levels showing the spectral broadening as the circulating power is increased. The bar above the optical spectra is the frequency span of high reflection of the FBG, approximately 50 GHz.

When a second amplifier was added, as in Figure 15(b), the laser typically self-organized its output to coherently couple the two optical beams when the polarization was properly matched as has been previously reported. At high power levels, the broadening could extend across the entire high reflection band of the FBG, as shown in Figure 17. The difference in path length between the two laser cavities led to a periodic modulation of the mode spectra, again in agreement with past data. Figure 17 shows two different typical examples with a ~10-cm and ~5-m mismatch. The spectral structure in the ~10-cm data is due to the ~2-GHz frequency modulation of the cavity loss spectrum associated with the length mismatch. The longer length mismatch produces ~40 MHz which is not resolved in this data. The addition of the second amplifier adds the effects of the length mismatch to the structure of the output spectra without qualitatively changing the broadening induced by the nonlinear optical interaction.

By changing the length mismatch between the two amplifier paths, we could generate spectral structure that varied from a few MHz to nearly 10 GHz. However, when the length mismatch became too small, typically <5 cm, coherent coupling became problematic. Such a length mismatch corresponds to spectral structure on the order of 10 GHz, a value approaching the 30- to 50-GHz frequency range of the FBG. In agreement with other results,[6,7] this indicates that when there are too few modes that are simultaneously resonant, other more random factors come in to play to prevent coherent coupling of the lasers.

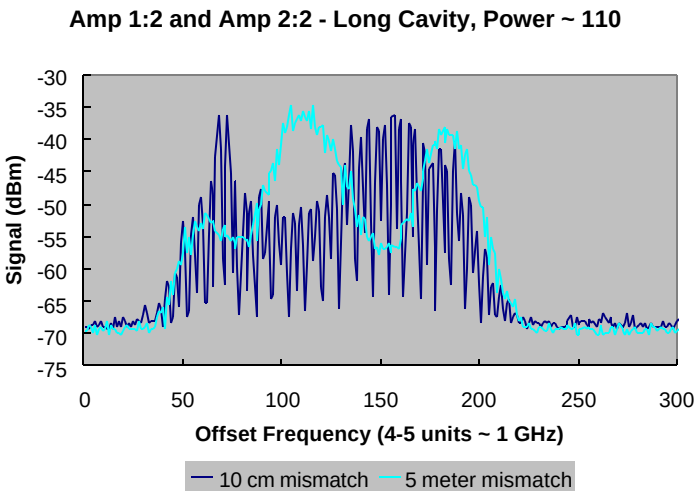

Figure 17(a). Optical spectra of two-laser, long cavity coherent output.

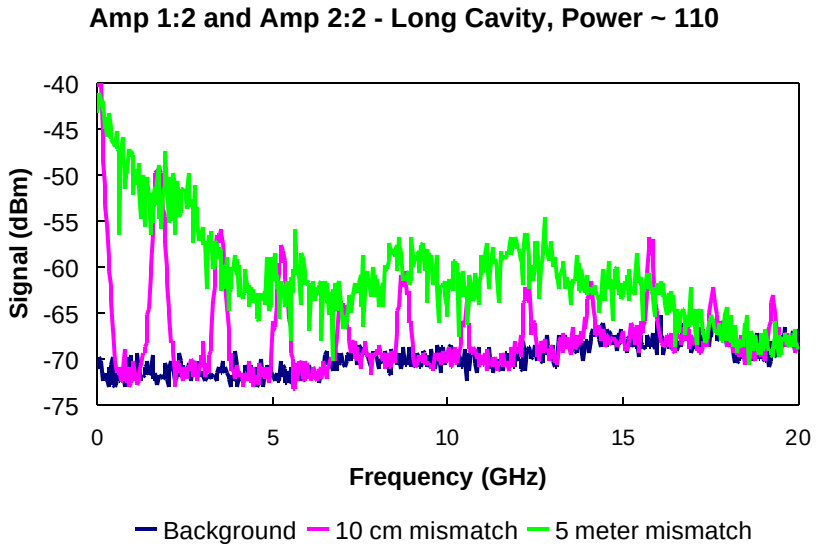

Figure 17(b). Power spectra of two-laser, long cavity coherent output.

Figure 17. Output power from a 2-laser baseline configuration with a 10-cm length mismatch between amplifier arms and when fiber is added to one arm to produce a 5-m length mismatch. Optical spectra (a) and power spectra (b) show broadening with the 10-cm length mismatch case also show the spectral structure associated with the length mismatch.

We also observed when running only 2 amplifiers that, regardless of path length difference, there was a high frequency modulation of 12 to 20 GHz to the spectra along with the lower frequency component that corresponded to the path length difference. Further, the power spectra features became generally weaker and broader when the frequency separation between peaks increased beyond approximately 5 GHz, corresponding to a path length difference of less than approximately 4 cm. Figure 18 compares the power spectra showing these changes. The relative dip in the spectra around 10 GHz does not seem to be related to SBS. We observed no backscattered signal that was not consistent with simple scattering off of intracavity connector interfaces. We also changed FBGs to see if the bandwidth of the gratings produced a measurable difference. We compared gratings with approximately 33-GHz and 50-GHz high reflection bandwidths. This change did not produce any obvious differences in the spectra.

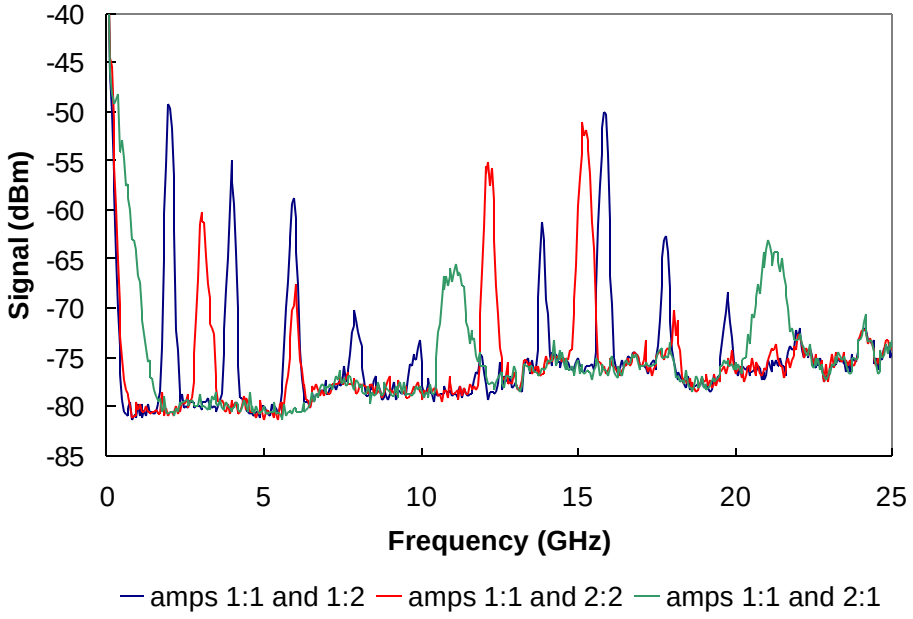

Figure 18. Power spectra when two of the four amplifiers are operating. Note how there is a modulation in the feature amplitudes at approximately 15 GHz in addition to the lower frequency modulation that corresponds to the length mismatch.

We also noted a new dynamics feature in the two-amplifier output when the lasers were operating in the pulsing regime. The time between pulses depended in a non-monotonic manner in the relative pumping levels of the two amplifiers. The relevant data is shown in Figures 19 and 20. Shown in Figure 19 is the output as a function of pump level when the two lasers are operated independently and when one amplifier is biased at a fixed level where it displayed pulsating output and the pump level of the second level is varied. Due to the coherence between the output of the two amplifiers, the combined output is much greater than the sum of the two outputs. Over the range of pump powers shown in Figure 19, the output consisted of pulsations that varied in period and peak power. Figure 20 shows the variation of these characteristics for the two laser combination. Note that the pulsation period initially increases for the coupled laser system as the pump level of the 2nd amplifier is increased even though the circulating power is much greater.

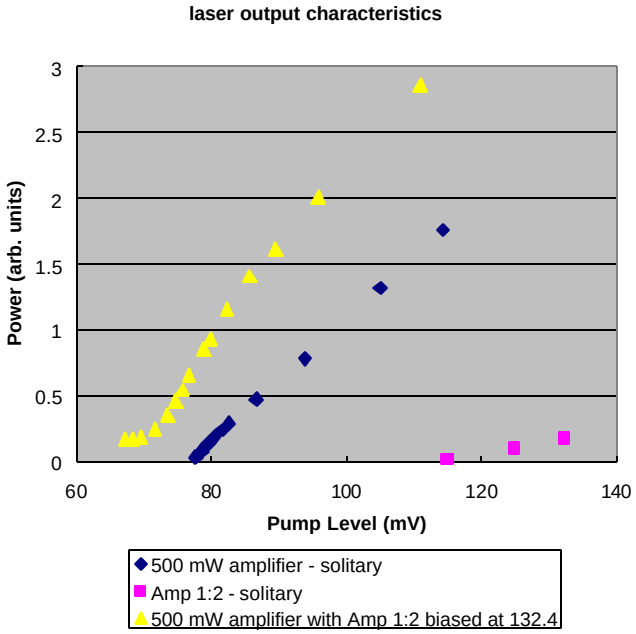

Figure 19. Output power as a function of measured pump level for the individual amplifiers in the two-amplifier configuration and when they are coherently combined. Amplifier 1:2 showed pulsating output at pump level 32 while the large amplifier and the combined output was pulsating over essentially this entire range of data points.

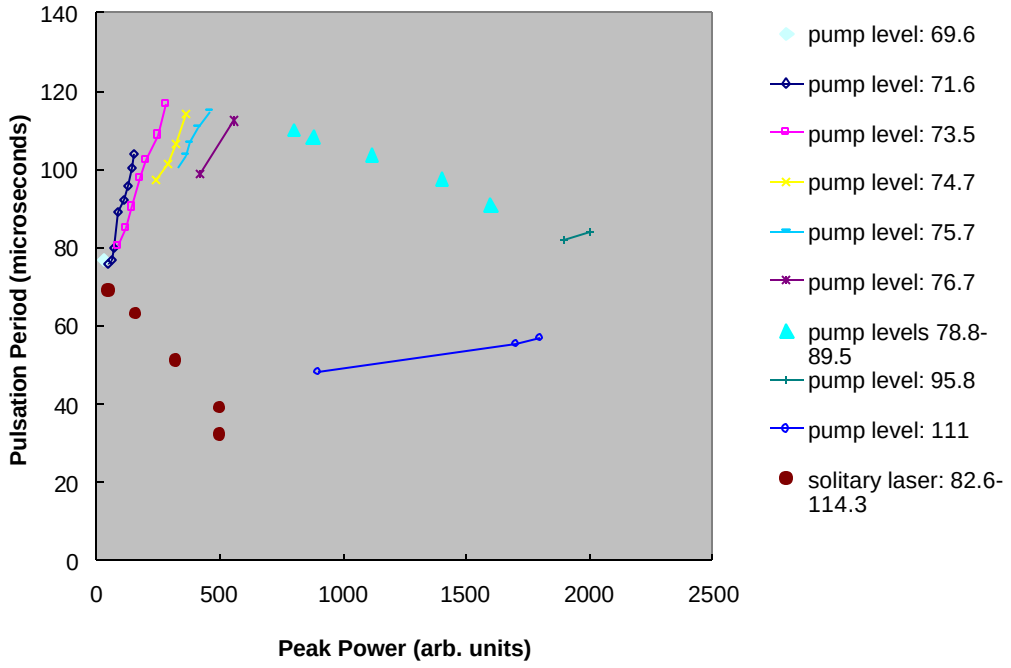

Figure 20. The pulsation period of the two-laser system as a function of the pulse power. One laser is biased at 132.4 where it displayed pulsating output of the combined cavity. The pump level to the large amplifier is varied over the range of pulsating output, with its output at a pump level of 80 equal to that of the first amplifier. Data points connected by lines were taken at the same pump level. Also shown, the brown circles are the data for the large amplifier as its pump level is varied and the other laser is unpumped. Compare with Figure 19.

The opposite behavior is displayed when the laser is operated independently. Here, the pulsation frequency decreases with increasing pump power. This latter behavior is consistent with typical of relaxation resonance frequency in simple class-B laser systems, though there is not the square root dependence on output power.

For several pump levels there was considerable variation in the peak power and period for a given pump level. This is shown by the connected series of data points in Figure 20 for several pump levels and a corresponding set of temporal data at one level in Figure 21. Note that amp 1:2 was pumped at a somewhat higher level that the previous data where it displayed

a stable output when operated in isolation. Clearly, one unstable laser can destabilize an otherwise stable partner. The increase in period with increased pulse amplitude is consistent with a longer recovery time from a more completely depleted gain medium. This may also explain the increase in the pulsation period with pump level. Because the coherent coupling reduces losses, the feedback to the gain medium is stronger. These stronger feedback pulses more completely deplete the combined gain media resulting in a longer pulsation period. However, more work is necessary to understand this unexpected dynamics.

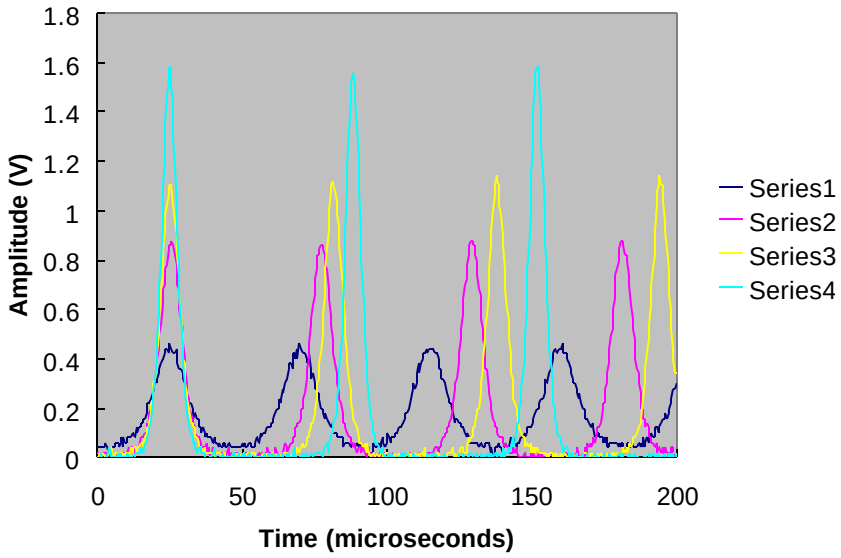

Figure 21. Time trace of a series of pulsating data for two coupled lasers taken when amp 1:2 was pumped to the level 165.2 and the 500-mW amp was pumped at 111.1. Compare with Figures 19 and 20.

Figure 15(b) is a schematic of the ring laser amplifier stage built around four independent Er-doped fiber amplifiers. The output from each amplifier is sent to an input port of a 2×2, 50/50 fiber coupler. A third 2×2, 50/50 fiber coupler is used to combine light output from the two fiber couplers. One output arm from this coupler is directed to the asymmetric, 90/10 fiber coupler or to a symmetric 50/50 coupler of the common path shown in Figure 14. The baseline configuration uses the 90/10 coupler with 10% of the light coupled out of the cavity. Again, port 2 of the fiber circulator is connected to a high-reflecting FBG that defines the bandpass of the circulating light. The light reflected back from the FBG passes out of Port 3 to a fiber polarizer. As we have discussed previously, the use of an intracavity element to enforce a single polarization simplifies the output spectrum and it was found that it also helps promote stable operation of the lasers in the coupled-cavity configuration. The polarized light output is input to the symmetric 1x4 fiber coupler shown in Figure 15(b). The outputs are directed through fiber polarization rotators, through fiber optical isolators and back into the fiber amplifiers to complete the ring cavity. There are three loss ports at the 2×2, 50/50 coupler outputs that can be used to monitor the degree of coherence. Another useful monitor port is the back of the FBG. Here, one monitors the light circulating in the cavity out of the bandpass of the grating. Due to the high intracavity gain, it is possible for the ring laser to go into spontaneous oscillation unless some care is taken to be sure that all of the fiber connectors are clean and the polarization rotators are adjusted so that circulating power is maximized for each cavity. The optical circulator and the optical isolators provide the non-reciprocal intracavity elements that enforce one-way propagation of light around the cavity. The port on the 10/90 output coupler could be used to insert an external signal into the cavity

In the base configuration, the mode spacing is approximately 6.24 MHz, corresponding to approximately 31.9 meters of fiber. Between the output of the final 2×2, 50/50 coupler and the input of the 1×4 coupler are approximately 10 meters fiber common cavity length. Each

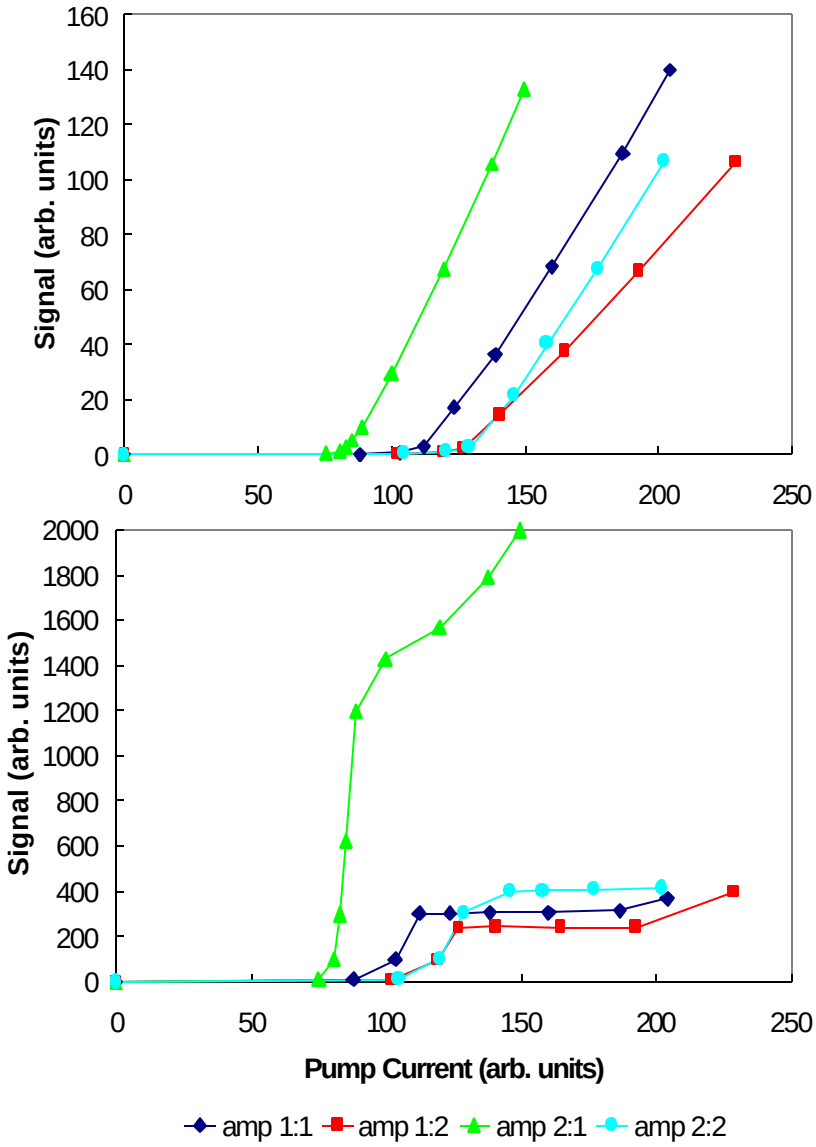

amplifier produced a somewhat different output when pumped individually. Figure 22

Figure 22. Upper plot – Relative output powers from each of the four constituent lasers when operated separately. Lower plot – Relative leakage power out of the back of the FBG. The scales of the two plots are not the same. The power out of the grating is a small fraction of the laser output power when pumped above threshold.

summarizes the output power as a function of input current to the diode pump lasers of the fiber amplifiers. Shown is the output at the output port and through the grating, the latter being a cavity loss. The power out the grating saturated near threshold, indicating that it measured the amplified spontaneous emission. We could use this output to determine the correct orientation of the fiber polarization rotators. When this output was minimized the cavities produced the proper polarization output. For the rest of the data the current to the amplifiers was set so that the output power in each of the lasers would be equal if uncoupled, at about 1.5x the threshold current level (corresponding to output powers around 100 to 120 in Figure 22). With no extra fiber there were relatively small differences in length among the four circulating paths. The path for amp 1:1 was longest with the amp 1:2 path approximately 1 cm shorter, 2:1 path approximately 4.2-cm shorter and 2:2 path approximately 9.5-cm shorter. Alternatively, one of the polarization rotators could be placed in the common cavity path to change the path length differences. Fiber can be readily inserted at many places into the cavity. We added fiber lengths to the individual cavities between the fiber polarization rotators and the intracavity optical isolators. Fiber was added to the common cavity before Port 1 of the optical circulator, between Port 2 and the FBG, or between the optical circulator and the fiber polarizer. Adding before the FBG caused the effective length to be doubled because the circulating light traverses this length twice. The difference between the two positions before and after the optical circulator was the optical power in the fiber due to losses in the circulator. This allowed investigations of different feedback power levels for otherwise similar configurations. Some important length-to-frequency conversions for the optical cavity are shown in Table 2.

Table 2. Approximate cavity length to frequency conversions.

1 cm ? 20 GHz	1 m ? 200 MHz	200 m ? 1 MHz
4.2 cm ? 4.8 GHz	5 m ? 40 MHz	800 m ? 0.25 MHz
9.5 cm ? 2.1 GHz	30 m ? 6.7 MHz	

As reported previously, in the base configuration the laser output was not steady. Figure 23 shows a typical time trace. Each amplifier had a tendency to operate on several adjacent longitudinal modes when operated independently and this behavior was exacerbated when more than one was operated together. The low-resolution optical spectra consisted of a few, typically 2-4, lines across the bandwidth of the FBG. The power spectrum of the photodetected signal of the optical output showed only a few lines up to 30 GHz with frequencies that varied on a scan-to-scan basis. The optical spectra were not reproducible. If an additional length (we could add lengths in increments of 1, 5 and 30 meters) of fiber is added to either the amp 1:1 or 1:2 path along with one other path, then the average output power became steady for short periods of time, after which it would switch to an oscillatory output at the inverse mode frequency. Figure 24 shows the typical long-term behavior when one meter of fiber is added to the amp 1:2 path while the other three remain unchanged. A detail of the oscillatory output is shown in Figure 23. Note how only the fundamental mode frequency now appears in the oscillation. Finally, if a second fiber patchchord is added to one of the other paths, the output became stable and good coherence was obtained. Figure 23 shows the output when the extra 5 meters is added to the 2:1 arm.

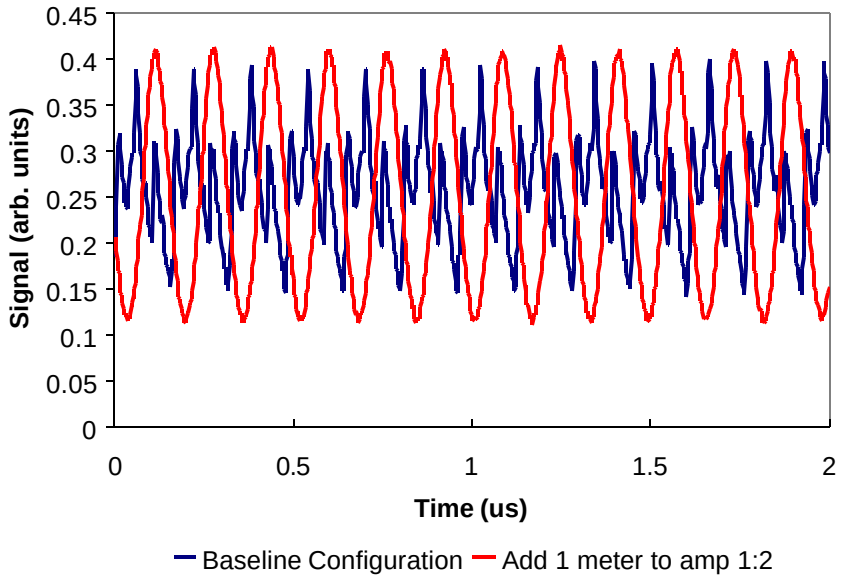

Figure 23. Output power from the 4-laser baseline configuration, dark blue curve, and when fiber is added to one arm. The ~6-MHz cavity mode spacing is evident in both and its harmonics are clearly evident in the baseline data.

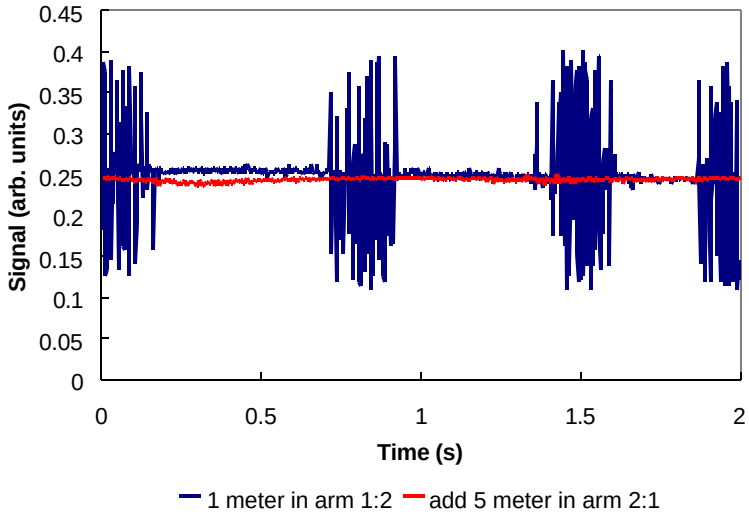

Figure 24. Longer term output characteristics for the 4-laser configuration with 1 m of extra fiber in the amp 1:2 arm (dark blue curve) , and when this configuration is modified by adding 5 meters of fiber to the amp 2:1 arm.

To try to get a better understanding of the output properties, we varied the length of the optical cavity. We previously reported that if sufficient extra fiber was introduced into the common cavity arm, the spectra became much richer while the coherence was not significantly degraded. Sufficient extra fiber was 200 meters before the circulator, with 100 meters being not enough to see the kinds of spectra that will be described below. After the circulator, even 400 m of additional fiber was insufficient to produce the richer spectra. The average power remained steady, but now there was significant temporal structure on time scales corresponding to the inverse cavity mode spacing and its multiples. For example, when 400 meters of extra fiber was added between Port 2 of the circulator and the FBG, effectively increasing the ring cavity by 800 meters of fiber, and 1 m was added in the amp 1:2 path and 5 meters was added in the amp 2:1 path, the temporal characteristics shown in Figure 25 were observed. Like the baseline configuration, the signal is nearly periodic but with the 4.1 microsecond period (0.24-MHz mode frequency) of the long cavity. When a ~10-kHz low pass filter is used on the optical signal, there are only random fluctuations of ~±5% on time scales of several seconds. Therefore, the array shows mode beating but not relaxation oscillation variations in the output.

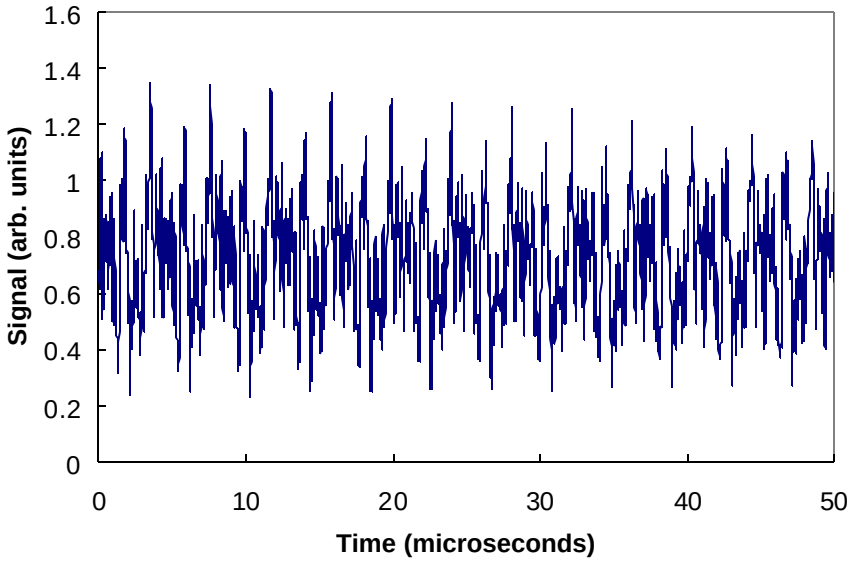

Figure 25. Time trace of a long cavity, four-amplifier configuration. The signal bandwidth is approximately 500 MHz.

Figure 26 shows a relatively low-resolution optical spectrum. The laser output is compared with the transmission spectrum of the FBG. The optical spectrum and the measurement of the transmitted signal through the grating are generated with the use of a DFB laser diode that has its temperature swept to change its output optical frequency. The DFB laser acts as the local oscillator for a heterodyne measurement to generate the optical spectrum. The optical spectrum is now a periodic set of peaks with a spacing of approximately 2.3 GHz. This fairly closely corresponds to the length mismatch between the paths for amps 1:1 and 2:2. This dense set of peaks is in stark contrast to the sparse and irregular set of peaks observed with the shorter cavity length.

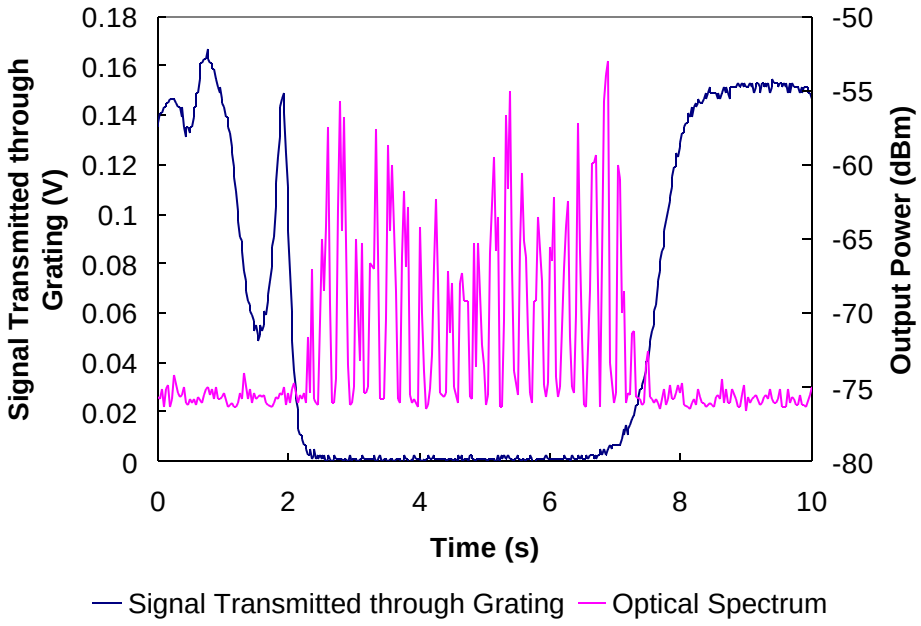

Figure 26. Optical spectrum corresponding to the time trace in Figure 25. The optical spectrum is superposed on the transmission spectrum of the FBG that defines the bandwidth of the ring cavity. The smallest length mismatch corresponds to a frequency spacing of ~2.1 GHz. The conversion from time of the frequency sweep to frequency is 1 s ~10 GHz (though not quite linear across sweep).

To verify that length mismatch produced the spacing, we swapped the 5-m fiber patchchord from the 2:1 path to the 2:2 path. Figure 27 shows the resulting optical spectrum. Now the separation is approximately 4.8 GHz, corresponding to the mismatch in length between 1:1 and 2:1. The 2.3 GHz and 4.8 GHz frequency offsets are the highest frequencies expected to be generated in the respective spectra based on the length mismatches. Each peak in the spectra varied apparently randomly in time, both in magnitude and in frequency, though the random frequency fluctuations were followed by all the peaks together.

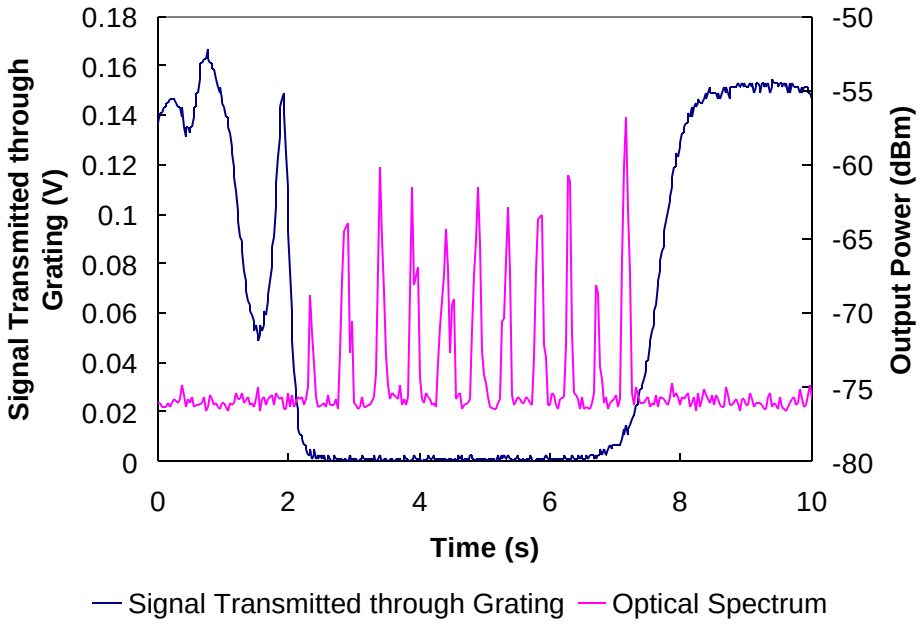

Figure 27. Optical spectrum showing the changes due to a change in the smallest cavity length mismatch relative to Figure 26. The optical spectrum is superposed on the transmission spectrum of the FBG that defines the bandwidth of the ring cavity. The smallest length mismatch corresponds to a frequency spacing of ~4.8 GHz. The conversion from time of the frequency sweep to frequency is 1 s ~10 GHz (though not quite linear across sweep).

Because of their low resolution, the optical spectra did not yield much detail. To observe greater spectral detail, we observed the output power spectra from the photodetector. Figure 28 shows the broadband power spectrum for the laser configuration corresponding to Figure 26. The features separated by 2.3 GHz are seen to be made up of a dense set of features that, in Figure 29, are shown to have dominant spacings of ~200 MHz and ~40 MHz, corresponding to the ~1-m and ~5-m length mismatches between the amp 1:1 path and the amps 1:2 and 2:1paths, respectively. Each of these peaks is further shown to be made up of a dense set of lines offset by the 0.24-MHz cavity mode frequency spacing (see Figure 30). These mode peaks also have structure, as shown in Figure 31. The structure is not evident for peaks at low frequency but becomes more pronounced as the frequency becomes larger. This indicates that the coupling between the cavity modes becomes weaker with greater frequency separation.

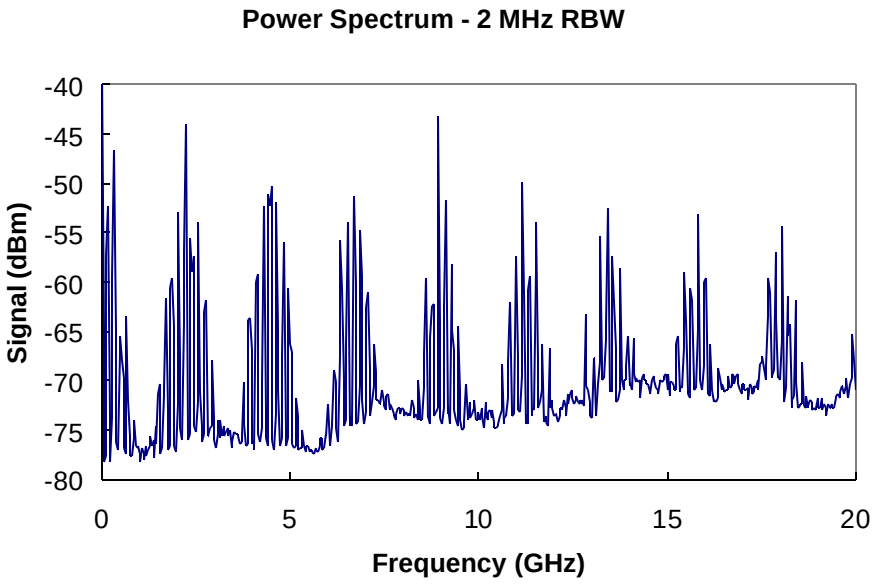

Figure 28. Power spectrum of the photodetected output of the laser array in the configuration corresponding to the optical spectrum in Figure 26. The resolution bandwidth (RBW) of the MSA is 2 MHz.

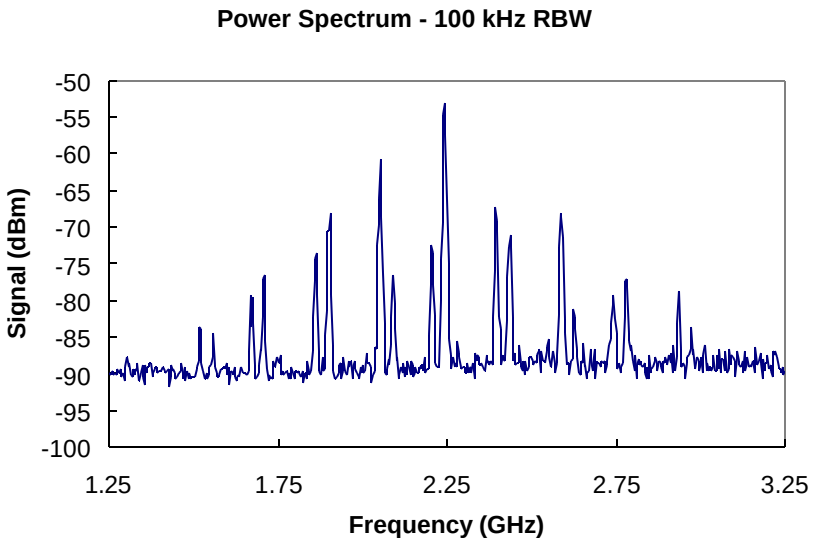

Figure 29. Detail of the power spectrum of the photodetected output of the laser array in the configuration corresponding to the optical spectrum in Figure 26. The RBW of the MSA is 0.1 MHz.

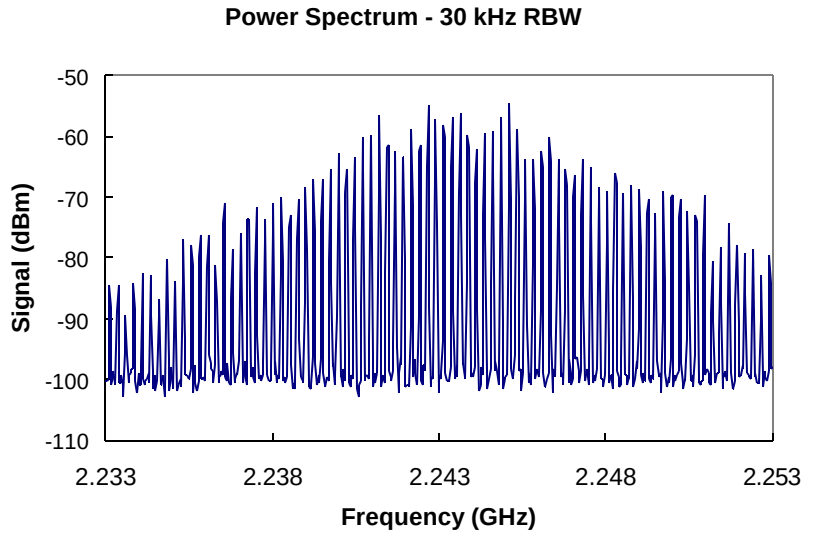

Figure 30. Detail of the power spectrum of the photodetected output of the laser array in the configuration corresponding to the optical spectrum in Figure 26. The RBW of the MSA is 30 kHz.

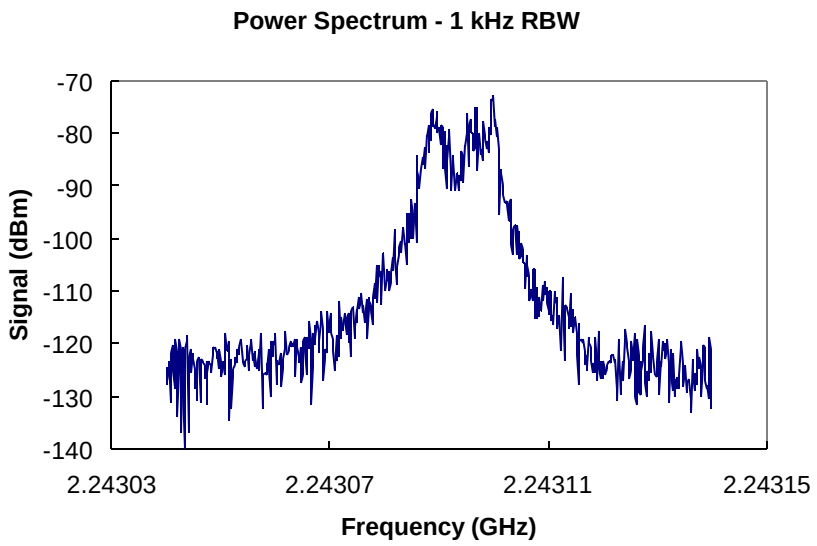

Figure 31. Detail of the power spectrum of the photodetected output of the laser array in the configuration corresponding to the optical spectrum in Figure 26. The RBW of the MSA is 1 kHz.

When a 30-m patchchord was added into one of the amplifier paths its associated ~7-MHz frequency spacing also became clear. Sometimes. if the length mismatches became sufficiently close to being multiples, the shorter mismatch, higher frequency spacing would be evident but the other would be suppressed. However, only when the smallest cavity length mismatch became sufficiently short, i.e., the ~1-cm mismatch between the amps 1:1 and 1:2 paths, was there deviation from the pattern of spectral spacings associated with length differences. Now the largest frequency spacing increased to 16 GHz, which is somewhat below the 20 GHz expected. We do not have an explanation for this frequency component but it correlates with the fact that we observed an anomalous 12 to 20 GHz component in the structure of the two-amplifier configuration.

The high coherence of the combined laser output is shown by comparing the output power from the laser with the output from the "loss" port of the final 2×2 coupler of the tree of couplers and the output from the back end of the grating. Table 3 summarizes a typical result

with the laser operating with the 90/10 output coupler configured to yield 90% feedback. All outputs are normalized to the signals with a solitary amplifier operating. The actual power that leaked through the grating was considerably smaller than the output or loss port powers for one amplifier. The two amplifier configuration was set up so that the beams were coupled in the same 2×2 coupler as the loss port measurement. The 8x increase in power from one to two amplifiers indicates that the losses form the extra fiber couplers make the one-amplifier configuration quite close to threshold at this pump level.[9] Coherent coupling reduces intracavity losses. Increasing from two to four amplifiers yields a 5x power increase that is closer to the 4x increase expected in the limit of pumping well above threshold. With all four amplifiers operating, greater than 95% of the circulating power is directed to the useful port of the 2×2 coupler for feedback and extracted power. It is important to remember that this is occurring even with the high frequency fluctuations in laser output due to the nonlinear mixing in the long cavities. When a 50/50 coupler is used, or even more dramatically when the 90/10 coupler is configured to yield 10% feedback, coherence is maintained in the four-laser configuration, even though the single laser configurations are now exhibiting only amplified spontaneous emission of spurious reflection points within the cavity and there is no wavelength or polarization control of the output. The good coherence is independent of whether there is a sparse or dense optical spectrum in the long cavity configuration. It is generally maintained even though the optical spectrum of the laser is varying over time with the changes in laboratory conditions. Over several hours of operation, the degree of coherence slowly drops but it can be restored by polarization adjustment. These results are potentially quite promising for the scaling of the system to large, high-power arrays. However, further work needs to be done to determine how the cavity length mismatches factor into the coherence in very large arrays. We have previously observed that the degree of coherence fluctuates strongly when the length mismatch in two-laser configurations drops to the cm range.

Table 3. Relative output power in four-laser configuration.

	Output	Loss Port	Grating
1 amplifier	1	1	1
2 amplifiers	8.2	0.6	0.5
3 amplifiers	21	2.4	1.2
4 amplifiers	43	0.9	1.4

When we added a fifth laser to the configuration, as in Figure 15(c), we anticipated that the stable broadening would continue and, perhaps, be observable with shorter cavities due to the higher circulating power levels. However, stable broadened spectra were not observed with the five-amplifier configuration. Instead, the laser displayed erratic spectra that only over long integration times would fill in to appear like the previously observed four-laser spectra. When we reconfigured the laser back to a four-laser configuration, but with different length mismatches (by a few cm) than before, this erratic behavior continued. Coherence remained quite good. The Japanese group has observed coherent coupling in a Michaelson-type configuration with eight lasers. Their structure also differed from ours in that all fiber connections were made by splicing fibers rather than using connectors and their gratings had a somewhat larger high reflection band of approximately 74 GHz.[7] These changes would have reduced parasitic intracavity reflections and increased the probability of overlap of all amplifier cavity spectra, respectively. They did not comment on the spectral stability of their output but did show that their coherent coupling efficiency could be modeled with a probability function of mode overlap.[7]

CONCLUSIONS

Work during the current program has demonstrated both the potential and some limitations of trying to investigate key physical parameters using a single flexible fiber apparatus. We have been able to reconfigure the apparatus to investigate polarization effects, nonlinear dynamics, and spectral characteristics of laser arrays ranging from two to five elements. We have observed a transition to a broadened spectral behavior that shows that cross-mode coupling using the basic, broadband fiber nonlinearity is the lowest threshold nonlinear optical interaction to produce strong changes in the output characteristics of the array. The spectral broadening limits the strength of the narrowband SBS interaction. Indeed, we observed no evidence of SBS in our data, even when the extra fiber was placed so that there would be counter propagating beams over long (~400 m) distances.

Unraveling the output spectra of multilaser arrays has proven to be a complex task. With the two-laser cavities we generate spectra that go from a sparse to dense transition as the circulating power and/or cavity length are increased. This transition occurs to the range where the nonlinear optical effects are calculated to be on the order of a few percent. The length mismatch enforces a modulation or periodicity on the spectra unless the length mismatch is so small that the frequency separation associated with the length mismatch comes within a factor of ~5 of the bandwidth of the FBG high reflectors. When there are four cavities present, we observe dense spectra with modulations corresponding to the different length mismatches that spans across the FBG bandwidth. These spectra can be fairly stable in time although quite often they showed large fluctuations on times of a second or less. While it is possible that these fluctuations were induced by parasitic etaloning effects in the cavity, we now believe that the stable spectra observed previously may have been due to a fortuitous combination of length mismatches between the various cavities such that the longer mismatches were near multiples of the shorter ones. We hypothesize that when this condition is not met for coupled cavities with more than two or three elements that the spectra will become erratic. We have tried to be careful about all of the fiber connections but it is possible

that small etalon effects become more important as the cavities become more complex. In a sense, the parasitic etalon effects would be acting upon the cavity in the same way as diverse length mismatches, introducing new phase relations for coherent coupling.

If the stable vs. fluctuating spectra is indeed a nonlinear optical effect arising from the various length mismatch relations, one is tempted to try and draw a connection between the spectral behavior that we observe and the phenomena of Arnold Tongues in nonlinear dynamics. Arnold Tongues are regions of periodic motion in an otherwise chaotic domain. The stable broadened spectra are consistent with periodic dynamics while the fluctuating spectra imply more complex dynamics. However, the time scales of the fluctuations that we observe, on the order of fractions of seconds to seconds are more consistent with random environmental changes. Perhaps, the spectral changes are manifestations of sensitivity to the "initial conditions," i.e., the exact configuration of the array down to the wavelength level. More work is required to determine if this speculation is pointing in the correct direction.

RECOMMENDATIONS

Considerable insight has been gained over the past few years into the output characteristics of intracavity-coupled fibers lasers. Because simple coupling with 50/50 fiber couplers can be augmented with coupling using multicore optical fibers [11,12] or even free-space coupling,[13] this technique is potentially scalable to very high power levels. The influence of nonlinear optical interactions and parasitic etaloning effects needs to be quantified. Highly fluctuating spectra are indicative of temporal fluctuations that are problematic for optical propagation in fibers due to nonlinear interactions. Though relatively weak, optical nonlinearities are known to generate a variety of characteristics including optical pulse compression and stretching, soliton pulse formation, and wavelength shifting, as well as induce catastrophic failure at points of imperfection.[10] Even with relatively low power levels, high intensities can be achieved when the beam is confined to single-mode propagation in a fiber. Single mode cross sections of 5×10^{-7} square centimeters (cm^2) are typical, yielding megawatt per square centimeter average intensity levels for Watt (W) incident power levels. Peak power levels can be orders of magnitude larger in situations where the laser output is pulsating, leading to fiber damage.

Therefore, it is critical to quantitatively understand the spectral characteristics of intra-cavity coupled fiber lasers and distinguish intrinsic mechanisms due to fiber characteristics and unavoidable length mismatches between the fibers in different elements of an array, from parasitic ones due to fiber or coupler imperfections that can, potentially, be eliminated through good fabrication practices. Experiments can be designed to distinguish these mechanisms using a flexible fiber laser array experimental apparatus such as the one described here. For instance, Figure 32 schematically shows a two-laser configuration where an intracavity etalon is deliberately introduced in one arm of the array. By controlling the etalon path length and the power circulating in the loop, one can quantitatively investigate parasitic etaloning effects. Such nonlinear work can be augmented by theoretical and modeling work to get a

better picture of the effects of the nonlinear optical interactions. Such work will identify the key physical mechanisms determining the coherent output from realistic fiber laser arrays.

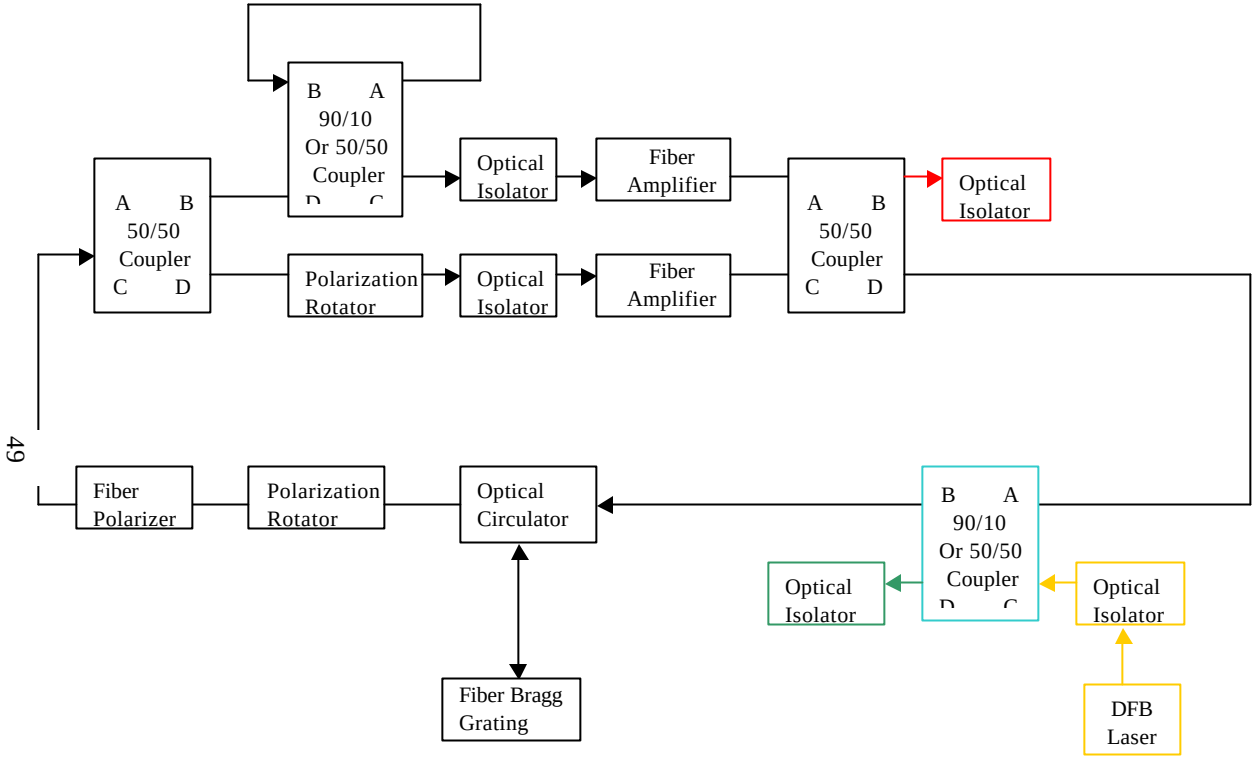

Figure 32. Schematic of a two-laser array configuration with an added coupler and fiber loop in one arm of the array. This coupler and loop mimic the effect of parasitic etaloning. The attenuation in the loop and the length can be adjusted, and the position in the optical ring can be adjusted to simulate a variety of parasitic etaloning effects.

REFERENCES

1. D.C. Brown and H.J Hoffman, "Thermal, Stress and Thermo-Optic Effects in High Average Power Double-Clad Silica Fiber Lasers," *IEEE J. Quantum Electron.* **37**, 207 (2001).

2. V.A. Kozlov, J. Hernandez-Cordero, and T.F. Morse, "All-fiber Coherent Beam Combining of Fiber Lasers," *Opt. Lett.* **24**, 1814 (1999).

3. T.B. Simpson, A. Gavrielides and P. Peterson, "Coherent Intra-cavity Coupling of Fiber Lasers," *Proceedings 2001 IEEE LEOS Annual Meeting*, vol. 1, 62.

4. D. Sabourdy, V. Kermène, A. Desfarges-Berthelemot, L.Lefort, A. Barthélémy, C. Mahodaux, and D. Pureur, "Power Scaling of Fiber Lasers With All-Fibre Interferometric Cavity," *Electronics Letters* **38**, 692 (2002).

5. A. Shirakawa, T. Saitou, T. Sekiguchi, and K. Ueda, "Coherent Addition of Fiber Lasers by Use of a Fiber Coupler," *Optics Express* **10**, 1167 (2002).

6. D. Sabordy, V. Kermène, A. Desfarges-Berthelemot, L.Lefort, A. Barthélémy, P. Even, and D. Pureur, "Efficient Combining of Widely Tunable Fiber Lasers," Optics Express **11**, 87 (2003).

7. A. Shirakawa, T. Sekiguchi, K. Matsuo, and K. Ueda, "Scalable Coherent Beam Combining of Fiber Lasers," in *Advanced Solid State Lasers*, J.J. Zayhowski, ed., OSA TOPS Vol. 83 (2003).

8. T.B. Simpson, *Fiber Laser Array*, Air Force Research Laboratory Technical Report AFRL-DE-TR-2001-1090, available from NTIC.

9. T.B. Simpson, A. Gavrielides and P. Peterson, "Extraction Characteristics of a Dual Fiber Compound Cavity," *Optics Express* **10**, 1060 (2002).

10. G.P. Agrawal, *Nonlinear Fiber Optics, 3rd Edition*, Academic Press, 2001.

11. P.K. Cheo, A. Liu, G.G. King, "A High-Brightness Laser Beam From a Phase-Locked Multicore Yb-Doped Fiber Laser Array," *IEEE Photonics Technology Letters* **13**, 439 (2001).

12. E.J. Bochove, P.K. Cheo, and G.G. King, "Self-Organization in a Multicore Fiber Laser Array," *Opics. Leters.***14**, 1200 (2003).

13. D. Sabordy, V. Kermène, A. Desfarges-Berthelemot, M. Vampouille, and A. Barthélémy, "Coherent Combining of Two Nd:YAG Lasers in a Vernier-Michaelson-type Cavity," *Applied Physics B* **75**, 503 (2002).

DISTRIBUTION LIST

DTIC/OCP
8725 John J. Kingman Rd, Suite 0944
Ft Belvoir, VA 22060-6218 1 cy

AFRL/VSIL
Kirtland AFB, NM 87117-5776 1 cy

AFRL/VSIH
Kirtland AFB, NM 87117-5776 1 cy

Official Record Copy
AFRL/DELO/Phillip Peterson 5 cys
3550 Aberdeen Avenue, Bldg. 400
Kirtland AFB, NM 87117-5776

Thomas B. Simpson, Project Officer 2 cys
The Titan Corporation/Applied Technology Sector
3394 Carmel Mountain Road
San Diego, CA 92121

(This page intentionally left blank.)